Dynamic Consolidation of Super Hard Materials

Wenbo Yang[1], G. M. Bond[2], Hua Tan[3], Thomas J. Ahrens[1], and G. Liu[2]

Period: October 1, 1988 to December 31, 1989

U.S. Army Research Office

Contract Number: DAAL03-88-K-0199

California Institute of Technology
Lindhurst Laboratory of Experimental Geophysics
Seismological Laboratory 252-21
Pasadena, CA 91125

Thomas J. Ahrens
Principal Investigator

---

[1]Lindhurst Laboratory of Experimental Geophysics, Seismological Laboratory, California Institute of Technology, Pasadena, CA 91125

[2]Department of Materials and Metallurgical Engineering, New Mexico Institute of Mining and Technology, Socorro, NM 87801

[3]Beijing Institute of Technology, P. O. Box 327, Beijing, People's Republic of China

UNCLASSIFIED
SECURITY CLASSIFICATION OF THIS PAGE

REPORT DOCUMENTATION PAGE

1a. REPORT SECURITY CLASSIFICATION: Unclassified	1b. RESTRICTIVE MARKINGS
2a. SECURITY CLASSIFICATION AUTHORITY	3. DISTRIBUTION/AVAILABILITY OF REPORT: Approved for public release; distribution unlimited.
2b. DECLASSIFICATION/DOWNGRADING SCHEDULE	
4. PERFORMING ORGANIZATION REPORT NUMBER(S)	5. MONITORING ORGANIZATION REPORT NUMBER(S): ARO 26171.3-MS-A
6a. NAME OF PERFORMING ORGANIZATION: California Institute of Technology; 6b. OFFICE SYMBOL (If applicable)	7a. NAME OF MONITORING ORGANIZATION: U. S. Army Research Office
6c. ADDRESS (City, State, and ZIP Code): Seismological Laboratory 252-21, 1201 E. California Blvd., Pasadena, CA 91125	7b. ADDRESS (City, State, and ZIP Code): P. O. Box 12211, Research Triangle Park, NC 27709-2211
8a. NAME OF FUNDING/SPONSORING ORGANIZATION: U. S. Army Research Office; 8b. OFFICE SYMBOL (If applicable)	9. PROCUREMENT INSTRUMENT IDENTIFICATION NUMBER: DAAL03-89-K-0199
8c. ADDRESS (City, State, and ZIP Code): P. O. Box 12211, Research Triangle Park, NC 27709-2211	10. SOURCE OF FUNDING NUMBERS: PROGRAM ELEMENT NO. / PROJECT NO. / TASK NO. / WORK UNIT ACCESSION NO.

11. TITLE (Include Security Classification): Dynamic consolidation of super hard materials

12. PERSONAL AUTHOR(S): Wenbo Yang, G. M. Bond, Hua Tan, Thomas J. Ahrens, and G. Liu

13a. TYPE OF REPORT	13b. TIME COVERED	14. DATE OF REPORT (Year, Month, Day)	15. PAGE COUNT
Technical	FROM 88101 TO 891231	900625	

16. SUPPLEMENTARY NOTATION: The view, opinions and/or findings contained in this report are those of the author(s) and should not be construed as an official Department of the Army position, policy, or decision, unless so designated by other documentation.

17. COSATI CODES		
FIELD	GROUP	SUB-GROUP

18. SUBJECT TERMS (Continue on reverse if necessary and identify by block number): consolidation, bonding, super hard materials

19. ABSTRACT (Continue on reverse if necessary and identify by block number)

Shock consolidation experiments were conducted via flyer impact on synthetic diamond (6-12μm) and cubic boron nitride (c-BN) (4-8μm) admixed with SiC whisker, Si_3N_4 whisker, SiC powder and Si powder contained in stainless steel capsules in the shock pressure range 10-30GPa. Scanning electron microscopy and transmission electron microscopy imaging of the samples revealed no plastic deformation or melting of diamond and virtually no deformation of c-BN, whereas the SiC and Si_3N_4 whiskers were extensively melted and recrystallized into bundle-shaped crystallites. In contrast, SiC powder mixed with diamond was also melted but demonstrated equant grain growth. A new mixture model of powder plus whisker materials is formulated on the basis of sphere-rod mixing and packing experiments. The model assigns excess porosity to the zone around whiskers and yields a better description of the energy deposition mechanism of the consolidation of powder-whisker systems. Some of the experiments employed Sawaoka's post-shock

(continued on reverse side)

20. DISTRIBUTION/AVAILABILITY OF ABSTRACT	21. ABSTRACT SECURITY CLASSIFICATION
☐ UNCLASSIFIED/UNLIMITED ☐ SAME AS RPT. ☐ DTIC USERS	Unclassified
22a. NAME OF RESPONSIBLE INDIVIDUAL	22b. TELEPHONE (Include Area Code) / 22c. OFFICE SYMBOL

DD FORM 1473, 84 MAR — 83 APR edition may be used until exhausted. All other editions are obsolete.

SECURITY CLASSIFICATION OF THIS PAGE
UNCLASSIFIED

annealing technique, in which the sample is sandwiched between two layers of a mixture of titanium powder plus carbon. Very well consolidated samples were obtained with post-shock heating under shock pressures of only about 12GPa. Micro-Vickers hardness values up to 27GPa were obtained for c-BN plus SCW at a low impact velocity of 1.45km/s with post-shock heating This hardness is similar to that obtained at a higher impact velocity of 1.95km/s without post-shock heating. To understand the post-shock heating process, one-dimensional time dependent temperature profile calculations were conducted for the sample and Ti+C layers. The calculated optimum Ti+C thickness is about 0.8-1.7mm at porosity of 40% for a typical sample thickness of 2mm. The heating and cooling time is a few milliseconds. Good compacts with Micro-Vickers hardness values up to 28GPa were also obtained upon shock consolidation of diamond plus Si admixtures.

TABLE OF CONTENTS

PREFACE

The following personnel at Caltech: W. Yang and Hua Tan; and at New Mexico Institute of Mining and Technology: G. M. Bond and G. Liu, contributed to the research results in this report. The assistance of J. Armstrong and P. Carpenter in the analysis of the shocked sample is appreciated.

LIST OF ILLUSTRATIONS

LIST OF TABLES

1. Introduction

Dynamic consolidation of such super-hard materials as diamond and (diamond-structured) cubic boron nitride (c-BN) initially in powder form with grain sizes in the range from 10-50μm shows some promise as a potential process for obtaining large quantities of technologically useful compacts. Single crystal powders of diamond are available from natural and synthetic sources (1), whereas c-BN single crystal powders are produced for abrasive applications with static high-pressure techniques (2). Recently several studies have been conducted in which single crystal powders, initially in the range of 60-70% of crystal density, have been consolidated to nearly crystal density by driving initial shocks of amplitudes in the range of 30GPa into sample containers within steel recovery fixtures. These shock pressures have been generated with both the impact of flyer plates accelerated with propellant and high explosive systems (3,4). In the case of diamond, scanning electron microscopy (SEM) images indicated that shock-induced interparticle bonding appears to result from local melting. Interparticle sliding upon compaction is inferred to produce this melting. Transmission electron microscopy (TEM) (5) of shock consolidated diamond demonstrates that this apparently melted material transforms, in part, to very fine polycrystalline diamond, an amorphous carbon phase, and graphite upon unloading and cooling. The presence of the graphite phase probably prevents this material from demonstrating exceptional small-scale strength in Vickers hardness tests. In contrast, single crystal c-BN compaction requires considerably higher shock pressures (33-77GPa) (6) to consolidate to nearly crystal density. This material demonstrates an impressive hardness of 50GPa approaching that of single crystal c-BN (66-75GPa). The consolidation mechanism in these experiments is not known although surface melting may also be occurring. Because of the irregularity and brittleness of the single crystals used in shock loading experiments, sound bonding between grains is not easy to obtain as the crystals tend to crack rather than change their shape plastically to fill the space between them.

Recently, Tan and Ahrens (7) reported that c-BN admixed with either Si_3N_4 (SNW) or SiC (SCW) whiskers formed hard uniform compacts upon shock compression to 22-23GPa, starting with mixtures which were ~70% of crystal density and contained 15 to 20% of whisker materials. Micro-Vickers hardness values as high as 50GPa were obtained for c-BN plus SNW mixture.

In the present study this work is extended to include studies of shock consolidation of diamond admixtures with SNW, SCW, SiC powder and Si powder. Samples were examined with SEM. In addition, a limited number of samples were studied by TEM. The TEM studies provided insight into the physics of the consolidation mechanism of whisker-cubic crystal mixtures and motivated a rod-sphere analog mixing model experiment. The result from the mixing experiment and a resulting simple model motivated modification of previous thermodynamic modeling methodology for shock consolidation. A new model of consolidation of cubic crystal-whisker mixtures is presented and a series

of revised thermodynamic calculations of the shock states achieved in the cubic crystal and whisker phases are conducted with this formulation. Finally, since many of our experiments employed layers of Ti+C surrounding our samples (first suggested by Sawaoka etal, 1988), we have developed a thermal model to describe the post-shock thermal annealing which takes place in the assembly.

2. Experimental Method

In addition to the SCW, c-BN and SNW used in previous experiments (7), we employed β-SiC single crystal powder and Si single crystal powder. The β-SiC single crystal powder is a product of Ibiden Co. Ltd. This material is reported by the manufacturer to have an average crystal diameter of 0.28μm. The main impurities, with a total mass of less than 1%, are Al, Fe, SiO_2, C and H_2O. The Si powder is commercially obtained with sizes of -325 mesh (less than 44μm). The impurities are also less than 1 wt%.

Two series of new experiments were conducted. The first series of experiments, which we carried out with a 20mm propellant gun, included: diamond powder mixed with SCW, SNW, SiC powder or Si powder in different mass ratios and initial porosities. Samples of pure diamond and SCW were also shock compressed to provide a comparision to the admixtures. The second series of experiments was conducted with a 40mm propellant gun. In these experiments, following the idea of Sawaoka (8), we consolidated the diamond (or c-BN) and SCW mixtures initially 2-3mm thick, which were sandwiched by a 0.8-1.5mm thick titanium and carbon black mixture. The purpose of the metallic titanium-carbon mixture is to provide a post-shock heat source to anneal the sample. The thermodynamics of this reaction and resultant heat flow is described in section 6.

All of the samples were prepared by the same method described in reference 7. A tantalum flyer plate was used to impact the sample assembly. The thicknesses of these plates for the 20mm gun and 40mm gun were 1.5mm and 2.6mm, respectively. The recovery method with momentum trap techniques, as previously described (7), was used.

3. Results

3.1. Diamond Powder Plus Silicon Nitride Whisker (SNW) Material

Our results are summarized in table 1. The estimated shock pressures in these experiments are about 25GPa. Of the five shots, four sample assemblies exploded, leaving a hole in the centre of the recovered Ta flyer plate. We infer that these explosions result from the expansion of N_2 gas produced by the reaction

$$3C + Si_3N_4 = 3SiC + 2N_2$$

At ambient pressure and temperatures higher than 1626K, the calculated Gibbs formation energy difference, ΔG, has negative values (Fig. 1). The Gibbs formation energy

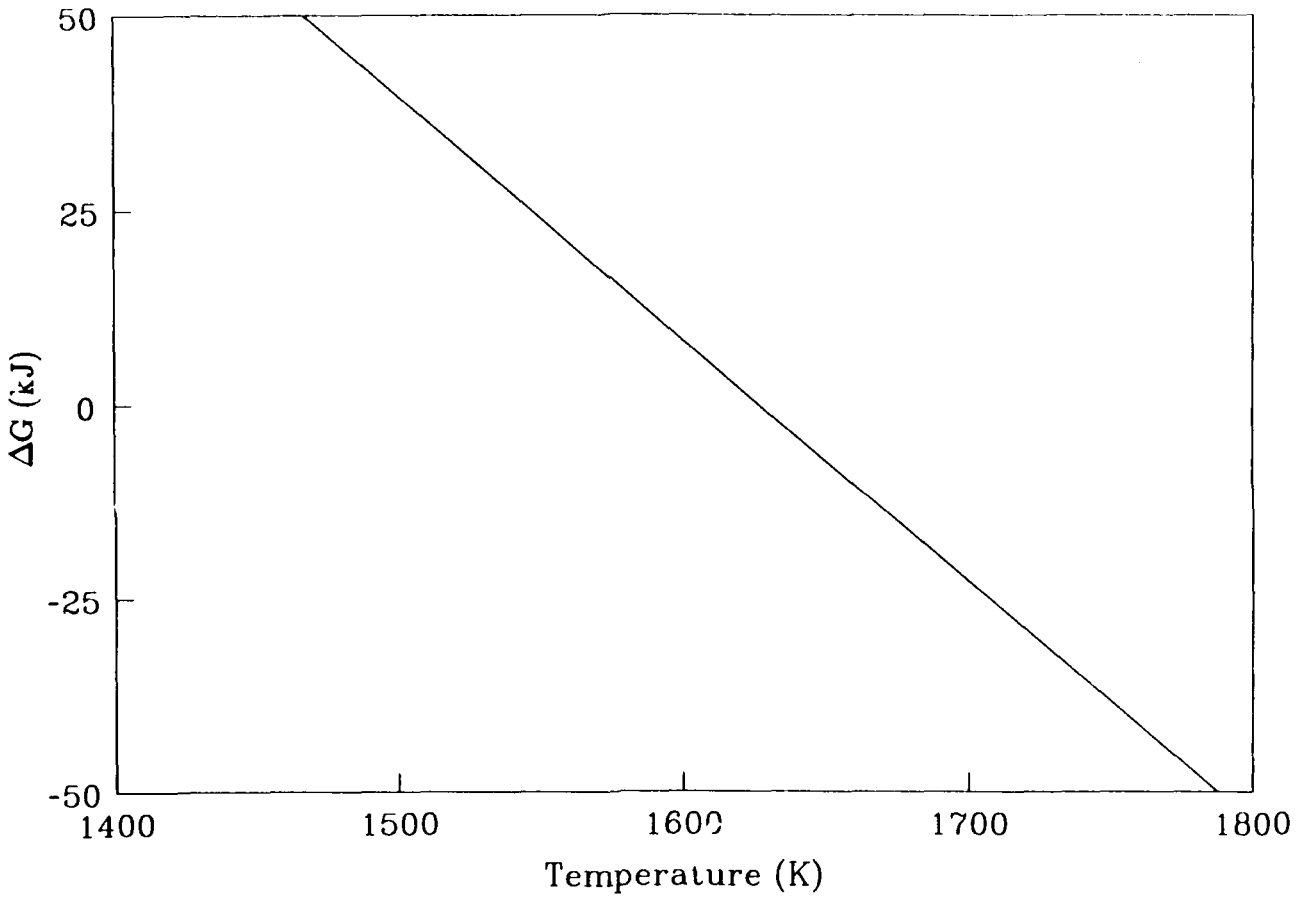

1. Calculated Gibbs formation energy difference ΔG vs. temperature of the reaction $3C + Si_3N_4 \rightarrow 3SiC + 2N_2\uparrow$.

Table 1. Diamond plus silicon nitride whisker (SNW) shock consolidation experiments

Experiments

Shot No.	Mass fraction (%)		Initial density (%)	Flyer velocity (km/s)	recovered results
	Diamond	SNW			
953	84	16	65	1.93	compacted,almost exploded
961	84	16	70	1.95	exploded,only a small piece recovered
962	80	20	66.6	1.97	friable
968	84	16	65.5	1.96	exploded
971	84	16	60	1.90(s.s.304)	exploded

Calculations

Shot No.	initial density (%)		P_H(GPa)	T_H(K)		T_p(K)		L(%)	
	Diamond	SNW		Diamond	SNW	Diamond	SNW	Diamond	SNW
953	68.3	53.5	22.2	1315	2173	1285	2173	8.8	94.5
961	72.6	59.8	25.5	1259	2173	1221	2173	8.1	83.1

at high temperature of SiC and Si_3N_4 are obtained from reference (9), and the Gibbs formation energy of diamond is from reference (30). According to our new admixture model, the SNW in these experiments will have a post shock temperature of 2173K (melting point) and nearly all (around 90%) the SNW in the sample will be shock melted.

The SEM images of sample pieces recovered from shots 953 and 961 are shown in Fig. 2. These demonstrate that the SNW has melted but do not indicate strong bonding between diamond particles although good consolidation can be seen in the very well mixed region. The fracture of individual diamond crystals can be seen clearly. A better consolidated sample might have been obtained if the content of SNW had been increased and the sample had been consolidated under a lower pressure.

3.2. Diamond Plus Silicon Carbide Whisker (SCW) Material

Most samples from these experiments were successfully recovered (Table 2). Two rather hard samples were obtained from shots 969 (Fig. 3a) and 973 (Fig. 3b) wuth 20 and 25 wt% SCW respectively. A very well consolidated sample was obtained from shot 1028 (Fig. 3d). For this shot, we added 30 wt% SCW to the diamond powder and expected that the additional SCW would protect the diamond grains from being fractured. This shot provided the best compact achieved with diamond. However the SEM images show that the diamond in all the present experiments is seriously fractured. Although the fusion bonding between diamond particles in some shots appears to be incomplete, the SEM images show that the SCW material is completely shock melted in all the experiments. In order to determine whether the Al_2O_3 shim was critical to the achievement of high quality compacts, we conducted shot 1007 (Table 2) without an Al_2O_3 shim at the impact end of the sample (Fig. 3c). No evidence of consolidation was obtained from the SEM image for this experiment. The lack of consolidation is inferred to result from the metallic spray from the sample container which contaminates the diamond plus SCW sample.

Although the fusion bonding between diamond particles in some shots appears to be incomplete, the SEM images indicate that the SCW material is completely shock melted and has flowed between the diamond particcles.

3.3. Diamond Plus SiC Powder and c-BN Plus SiC Powder

Unlike our previous results for shock compaction of c-BN plus SCW, no consolidated c-BN plus SiC powder mixture sample was obtained. The major results are listed in Table 3.

Diamond plus SiC powder also does not consolidate with the present method and the results are considerably less successful than the diamond plus SCW experiments.

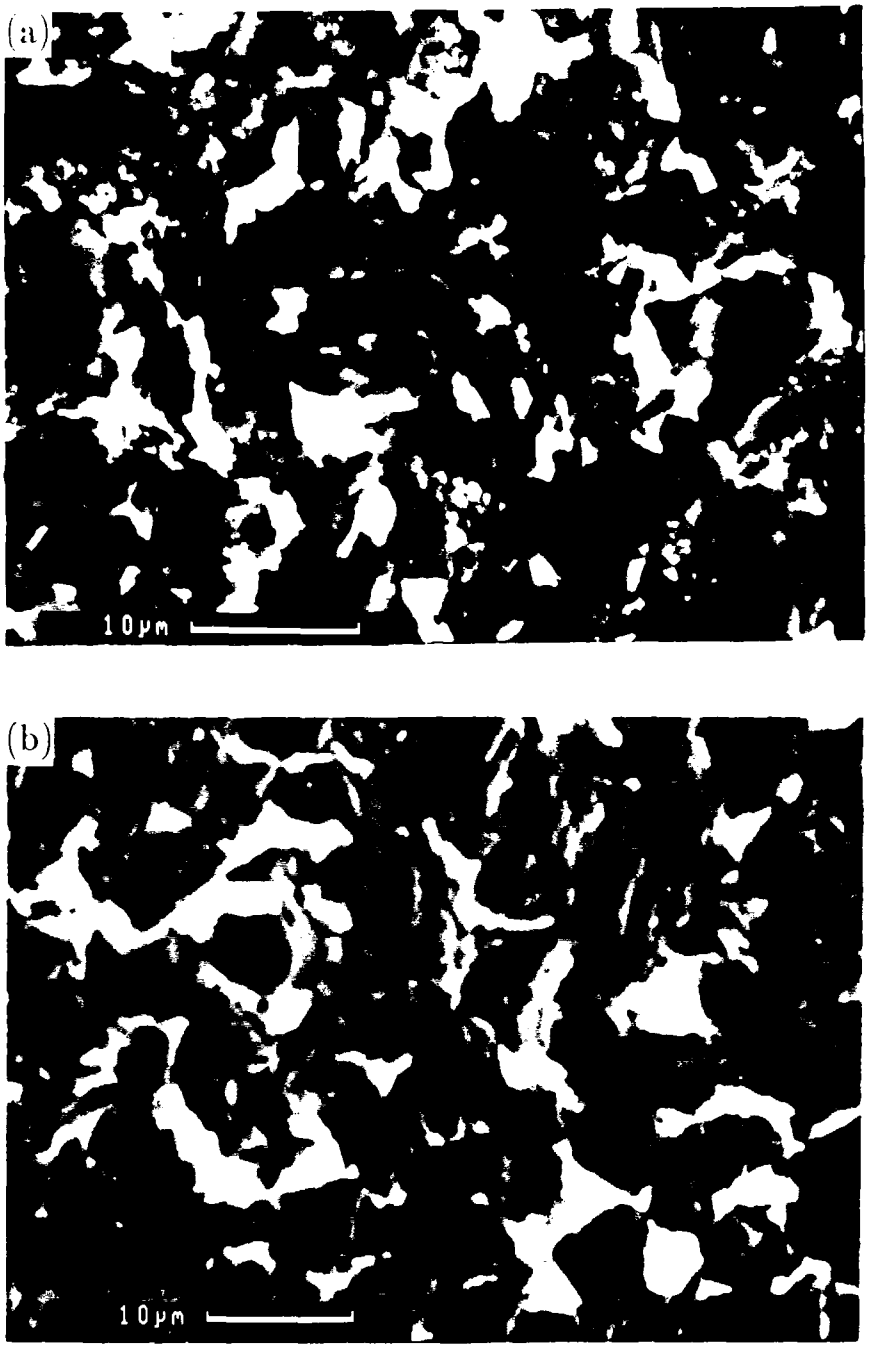

2. SEM images of diamond plus SNW. (a) Shot 953; (b) Shot 961. The light-colored phase is silicon nitride whisker (SNW).

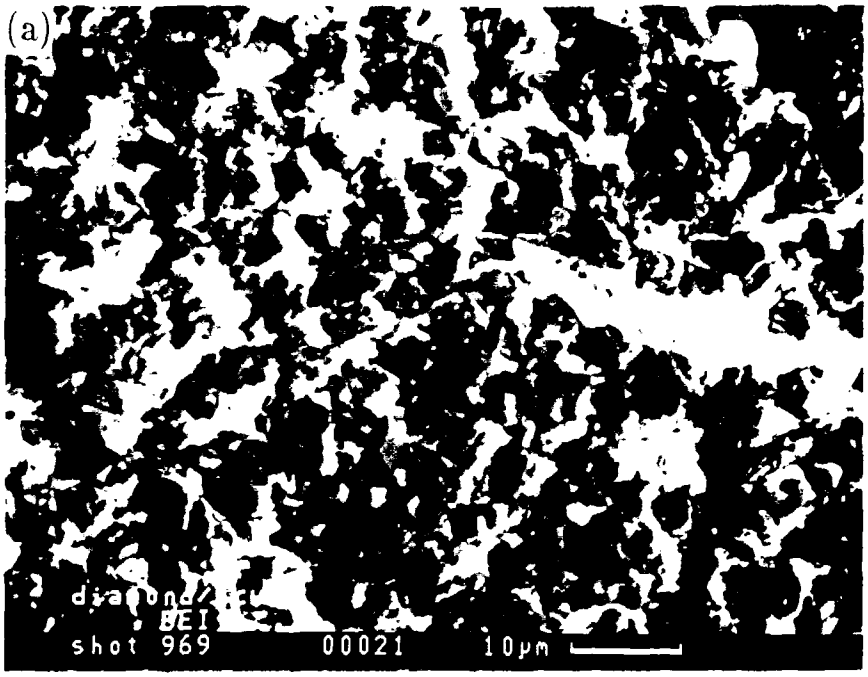

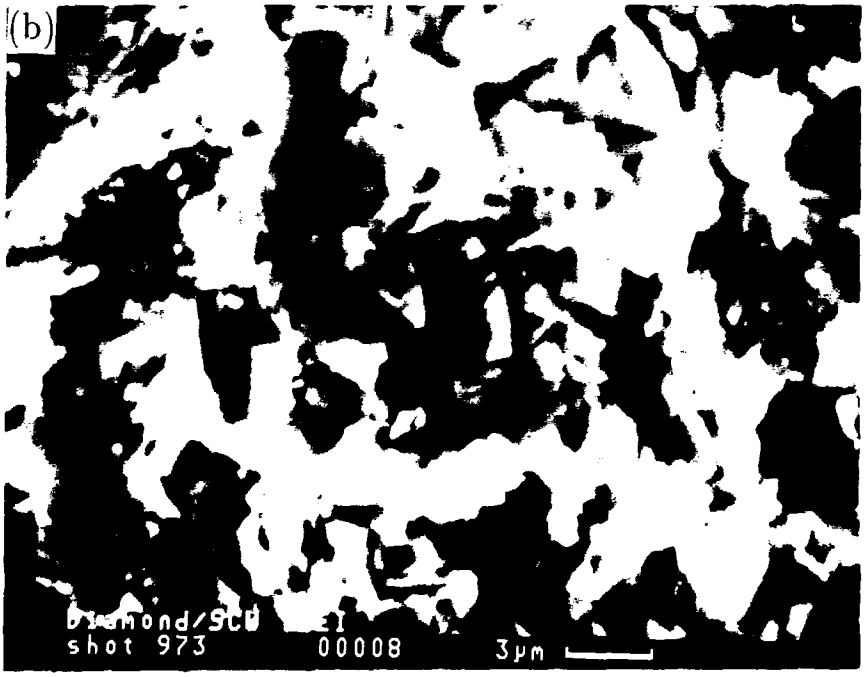

3a,b SEM images of diamond plus SCW. (a) Shot 969; (b) Shot 973;

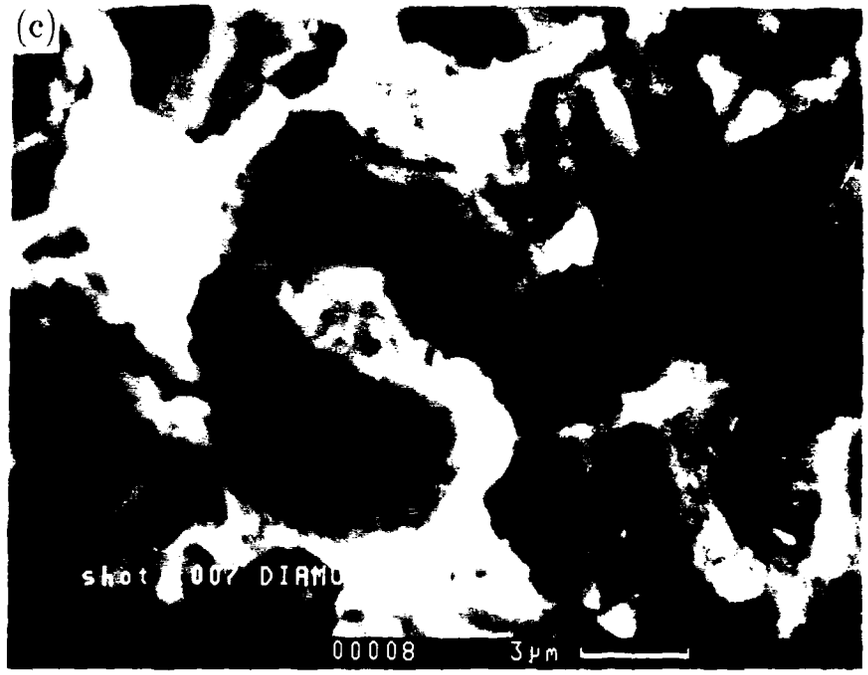

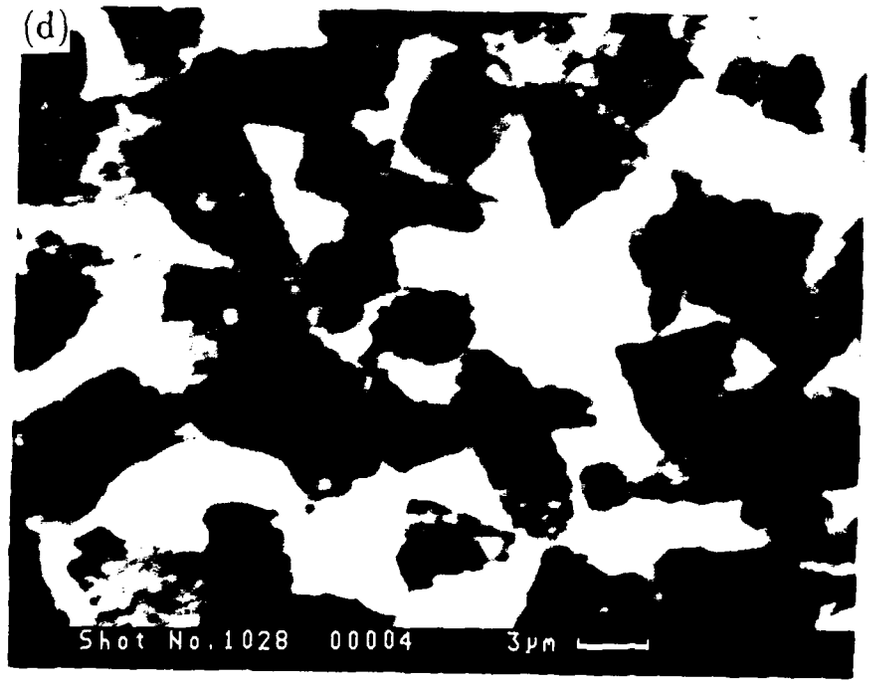

3c,d (c) Shot 1007; (d) Shot 1028. (d) (light-colored phase) shows very well consolidated features. The fractures of diamond (dark phase) grains can be clearly seen in all the images. The light-colored phase is silicon carbide whisker (SCW).

Table 2. Diamond plus silicon carbide whisker (SCW) shock consolidation experiments

Experiments

Shot No.	Mass fraction (%)		Initial density (%)	Flyer velocity (km/s)	recovered results
	Diamond	SCW			
966	80	20	70	1.99	friable
969	80	20	60	1.90	compacted,hardness ~ steel,cracks
970	100		55	1.90(s.s.304)	friable
973	75	25	60	2.00	consolidated,hardness ~ WC,numerous cracks
1007	75	25	60	1.85	uncompacted
1028	70	30	60	1.95	consolidated,scratches sapphire

Calculations

Shot No.	initial density (%)		P_H(GPa)	T_H(K)		T_p(K)		L(%)	
	Diamond	SCW		Diamond	SCW	Diamond	SCW	Diamond	SCW
969	71.0	54.2	22.3	1218	2937	1189	2836	7.7	37.1
973	68.2	45.2	20.7	1237	2963	1209	2963	8.1	49.2

Table 3. Cubic boron nitride (c-BN) plus SIC powder shock consolidation experiments

Shot No.	Mass fraction (%)		Initial density (%)	Flyer velocity (km/s)	recovered results
	c-BN	SiC			
980	80	20	70	1.89	friable
982	80	20	60	1.96	hard,many cracks
983	75(Diamond)	25	60	2.0	recovered a small friable piece
1001	80	20	70	1.76	still powder
1002	75	25	70	1.56	still powder
1003	75	25	70	2.03	friable

3.4. Diamond Plus SCW Sandwiched with Ti+C

These experiments were conducted with a 40mm gun rather than a 20mm gun and employed samples which contained three layers: Ti plus C, diamond plus SCW, and Ti plus C. We chose a stoichiometric ratio of Ti to C equal to that in TiC of 3.99 to 1. The major results of the experiments are presented in Table 4. Notably, the impact velocity of the 2.6mm thick Ta flyer plate is much lower than those used in 20mm gun experiments (see Table 2) and a longer shock duration is employed. The recovered samples indicated a well consolidated appearance with very few cracks. Micro-Vickers hardness tests were conducted and resulted in a hardness of about 10GPa. SEM images (Fig. 4) demonstrate that the whisker materials are not very well dispersed in the diamond powder and there are cracks in the SCW rich zones. Moreover, the diamond powders, although well consolidated in what appears to be melted SCW, are unexpectedly severely cracked. Both the lack of ideal diamond-SCW dispersion and excessive diamond cracking probably interfere with obtaining optimum consolidation.

3.5. c-BN Plus SCW Sandwiched with Ti+C

Two shots were fired and the results are listed in Table 5. The Ti+C layer is ~0.8mm thick and the impact velocity is 1.35 to 1.45km/s in these shots. The recovered sample of shot 787 is very well consolidated. The bonding between c-BN particles by the SCW texture is very sound. This sample is very hard and tough and the sample container was opened via surface grinding. The silicon carbide grinding wheel sparked brilliantly whenever it contacted the sample. A tungsten carbide probe deposited material onto the sample surface rather than scratching the sample. These observationsare compatible with our previous shock compaction results of non-sandwiched c-BN plus SCW mixture performed with a 20mm gun, in which a higher impact velocity (1.95km/sec.) and initial density (~70% of crystal density) were used. Micro-Vickers hardness test shows the sample has a hardness of about 27GPa. We also measured the sample's density and its longitudinal wave velocity. The results are given in Table 6. It appears that this sample achieved the crystal density of the mixture within the stated uncertainties.

In comparison with shot 787, the recovered sample of shot 786 shows a relatively lower hardness and less consolidation, due to the lower impact velocity. We thus expect better consolidation with a slightly higher velocity. Radial cracks still exist in the recoved samples, which we believe are caused by the radial stress from the side rarefaction wave after shock wave passage. We believe these cracks can be eliminated by use of a star shaped flyer plate (10).

SEM images are shown in Fig. 5 which demonstrate sound bonding between c-BN particles. Notably, no cracks can be seen in the c-BN crystals. This implies the c-BN single crystals are stonger than the man-made single crystal diamond upon shock consolidation.

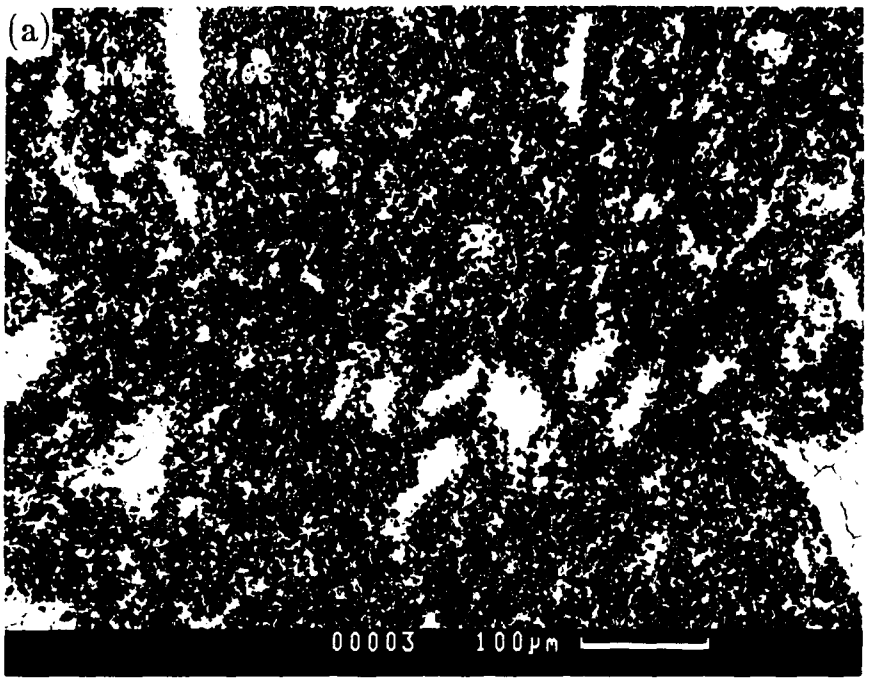

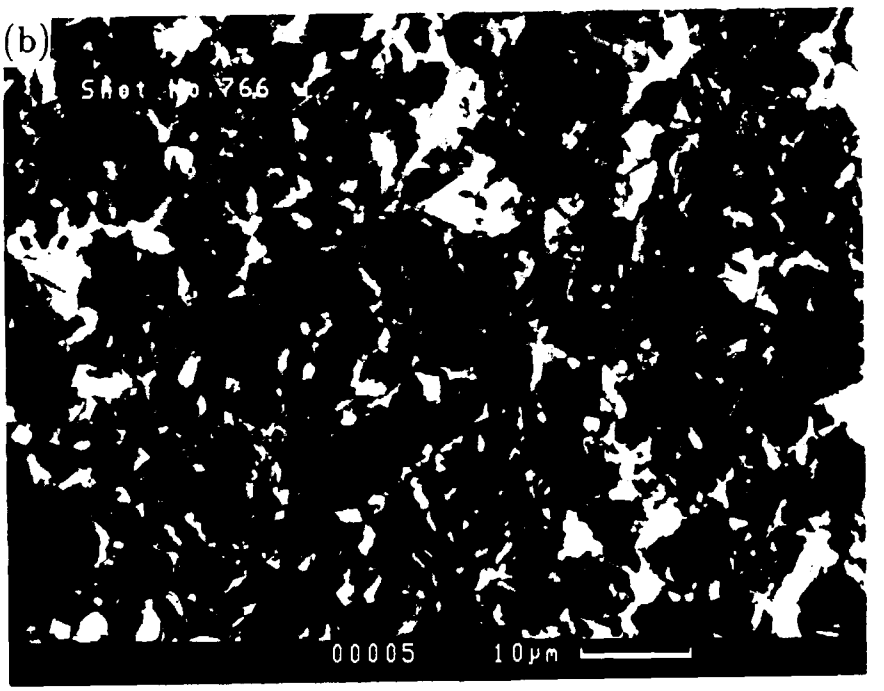

4a,b. SEM images of diamond plus SCW sandwiched with Ti+C. (a) and (b) show the cracks in the SCW rich regions and the heavily pulverized diamond grains in the SCW deficient region of Shot 766.

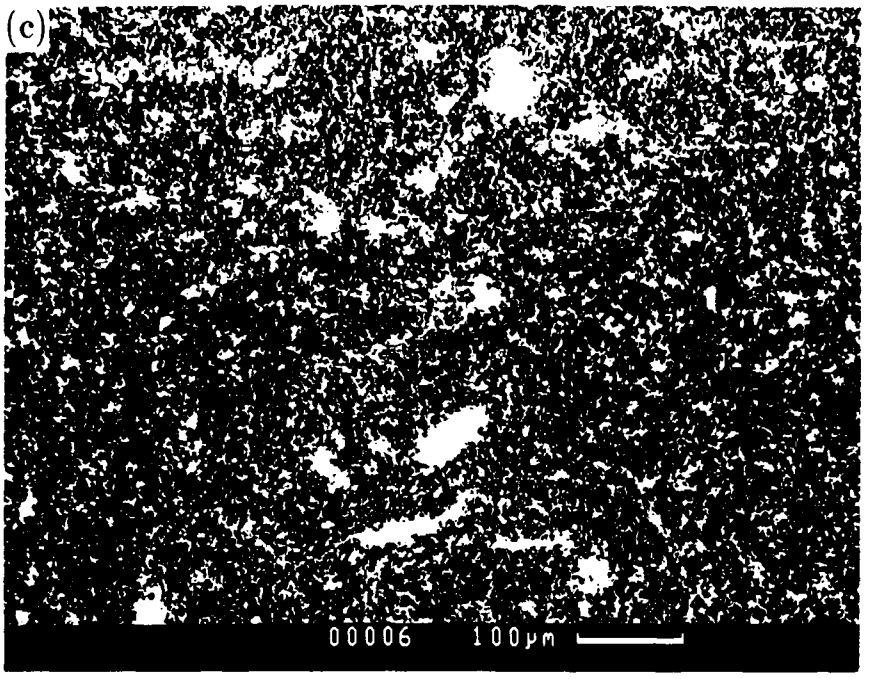

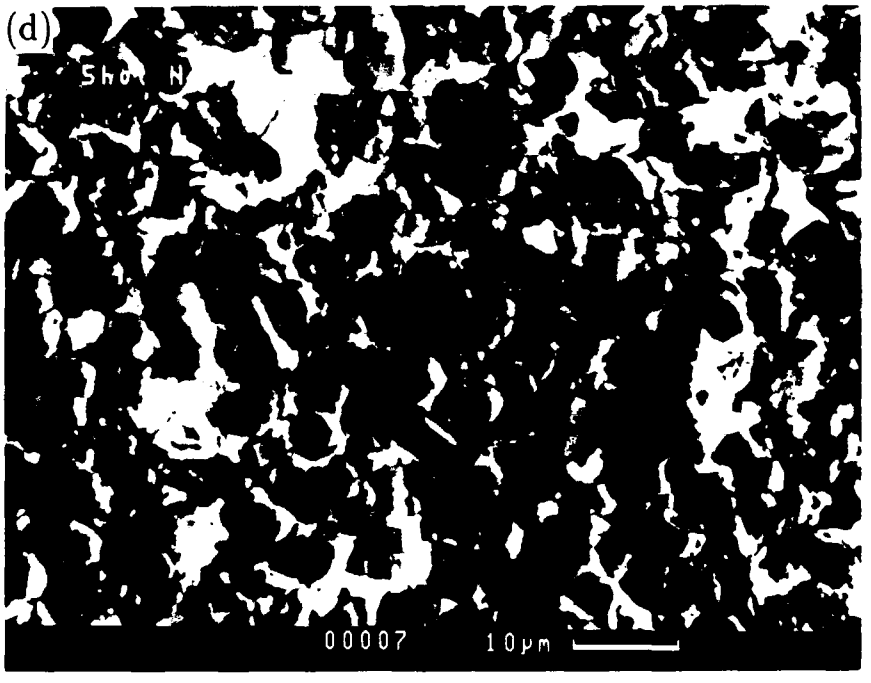

4c,d (c) and (d) show that similar consolidation features occurred in Shot 766 to those in Shot 767.

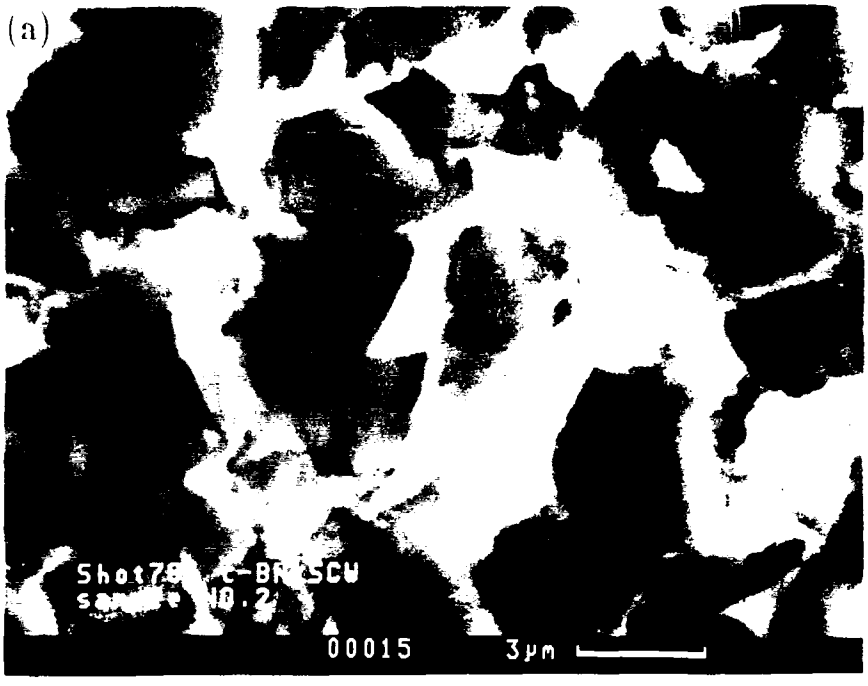

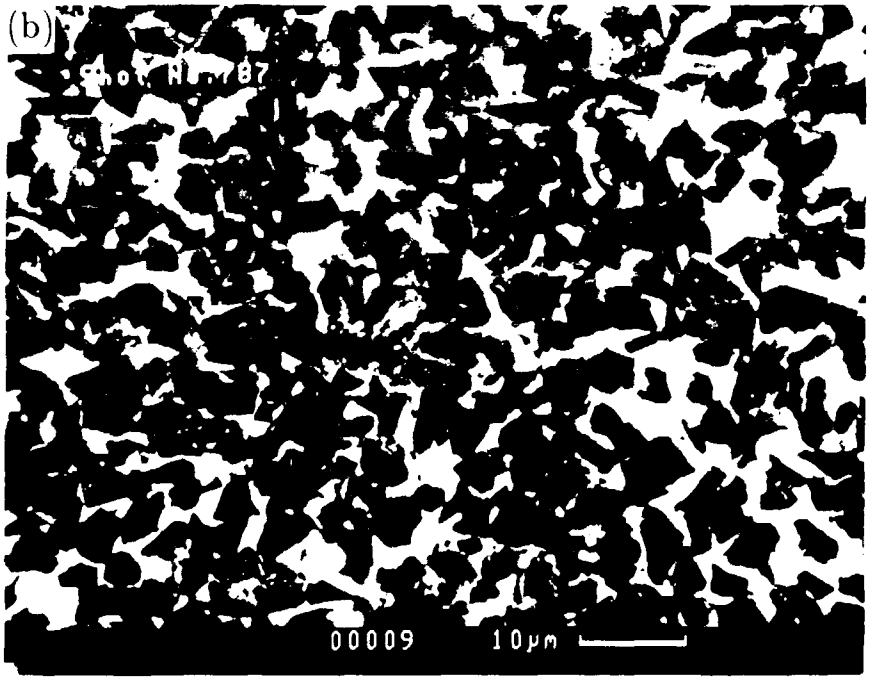

5. SEM images of c-BN plus SCW sandwiched with Ti+C. (a) Shot 786; (b) shows very nice texture of SCW in Shot 787. Note that no cracks can be seen in the c-BN grains.

Table 4. Diamond plus silicon carbide whisker (SCW) sandwiched with Ti+C, shock consolidation experiments

Experiments					
Shot No.	Mass fraction (%)		Initial density (%)	Flyer velocity (km/s)	recovered results
	Diamond	SCW			
766	80	20	60	1.30	hard,large sample recovered with a few cracks
767	80	20	60	1.42	same

Calculations									
Shot No.	initial density (%)		P_H(GPa)	T_H(K)		T_p(K)		L(%)	
	Diamond	SCW		Diamond	SCW	Diamond	SCW	Diamond	SCW
766	71.0	54.2	10.9	833	1650	820	1592	3.8	18.1
767	71.0	54.2	12.6	894	1831	876	1776	4.3	21.0

Table 5. Shock consolidation results,c-BN plus SCW sandwiched with Ti+C

Experiments					
Shot No.	Mass fraction (%)		*Initial density (%)*	Flyer velocity (km/s)	recovered results
	c-BN	SCW			
786	75	25	60	1.35	hardness~hardened steel,few cracks
787	75	25	60	1.45	hardness~harder than WC, few cracks
808*	75	25	60	1.36	unconsolidated

Calculations									
Shot No.	initial density (%)		P_H(GPa)	T_H(K)		T_p(K)		L(%)	
	c-BN	SCW		c-BN	SCW	c-BN	SCW	c-BN	SCW
786	68.1	45.3	10.3	890	2045	877	2026	4.8	24.5
787	68.1	45.3	11.6	947	2255	928	2225	5.4	27.7

* not sandwiched with Ti+C.

Table 6. Elastic Moduli of Super Hard Materials

Crystal (Structure)	bulk modulus (GPa)	shear modulus (GPa)	density (g/cm^3)	longitudinal wave velocity (km/sec)
C (Diamond)	441	532	3.51	18.1
BN - (Diamond)	369	445	3.489	16.6
SiC (Zincblende)	200	173	3.122	11.8
(theoretical) 4:BN + 1 SiC	276	342	3.39	14.7
(observed) 4:BN + 1:SiC			3.449±0.19	12.27±0.58

3.6. Attempted Shock Compaction of SCW

Three experiments were conducted. Two of these totally failed. A third shot (shot 1004) was carried out without an Al_2O_3 shim at the impact end of the sample (Table 7).

SEM analysis of a small aliquot sample shows that these whisker materials are not compacted, and many of them still retain at their original texture (Fig. 6). Calculations employing the shock wave data in reference (23) show that, with an impact velocity of 1.95km/sec., the initial shock pressure for shot 1004 is about 13GPa. This pressure may be below the Hugoniot elastic limit of SCW. Only a very small amount of deformed sample material was found in the outer part of the recovered sample.

3.7. Diamond Plus Si Powder

Five experiments were conducted (Table 8). All of them were recovered and very hard samples were obtained. The resulting samples can scratch glass or single crystal Al_2O_3. Shot 1024 has a Micro-Vickers hardness of 28GPa. SEM images (Fig. 7) demonstrate that all the Si powders are shock melted. Very sound bonding between diamond crystals by melted Si can be seen. As in other experiments with synthetic diamond powders, the diamond crystals are pulverized by shock loading. Shot 807 was performed with the 40mm gun and sandwiched by Ti plus carbon black. The impact velocity is much lower (1.18km/sec.) compared with other shots.

4. Transmission Electron Microscopy Results

The major objective of the TEM study of the present samples was to determine whether the SiC whisker and powder and/or diamond had melted along the interfaces, and whether diamond-silicon carbide reactions had occurred at the interface between phases. We also expected to determine whether cracks were present between phases, and in which phase shock induced cracks occurred.

Diamond samples consolidated with both SiC powder and SCW were sliced (to 0.5mm thick), and then polished via a two step abrasion with diamond paste to reduce their thickness down to 70-200μm. After polishing, the samples were ion milled down to electron transparency (~10-100nm) thick in a Commonwealth Scientific STATMMI-2 argon-ion milling apparatus. These foils were in turn examined in a 100keV JEOL Model 100C TEM.

Both bright-field (Fig. 8a) and dark-field images (Fig. 8c and d) of the diamond admixed with the initially 0.28μm β-SiC powder from shot 983 (see Table 3) demonstrate that the SiC has completely recrystallized. Although a few grains appear to be as large as ~100nm (0.1μm) virtually all the single crystal domains are now in the size range of 30nm or smaller, and the crystal orientation of the recrystallized SiC appears to be truly random. Moreover the boundaries between what we assume to be recrystallized β-SiC and the diamond are smooth and in several cases are straight, indicating that interpenetrative motion between the diamond and SiC phase has been minimal. We infer that

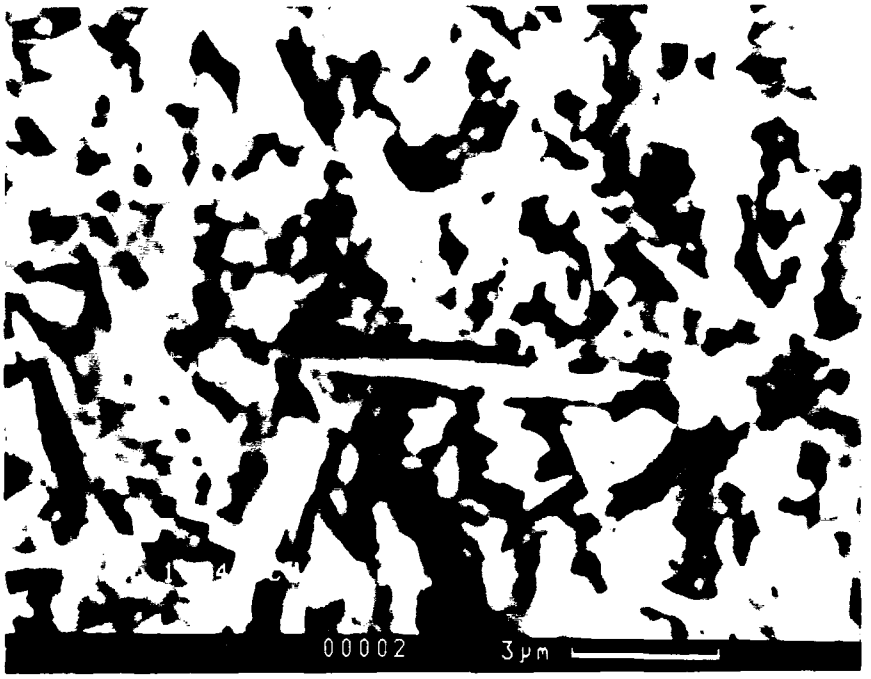

6. Many SCW retain their original form after a 13GPa shock compression (Shot 1004).

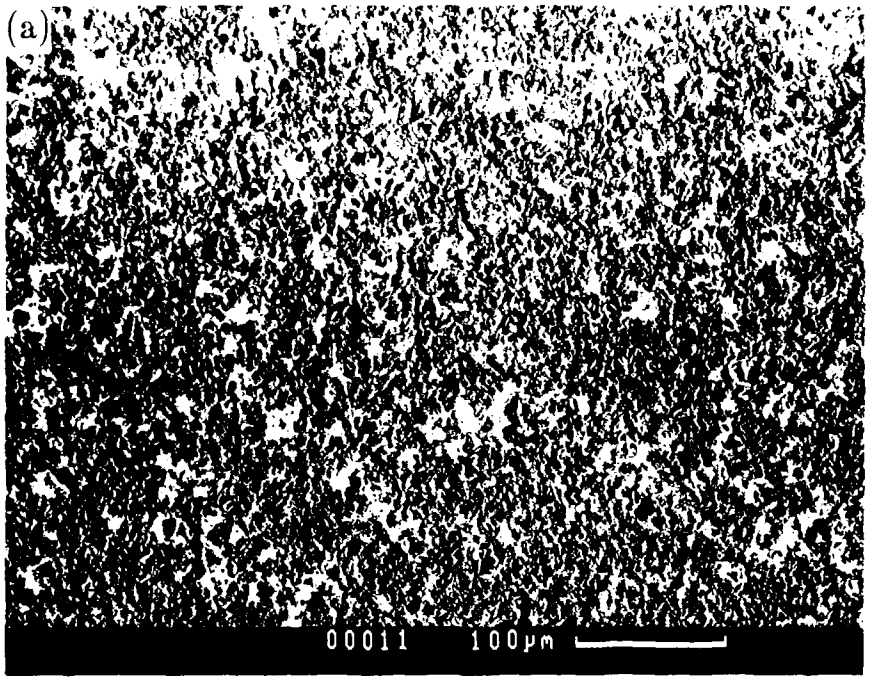

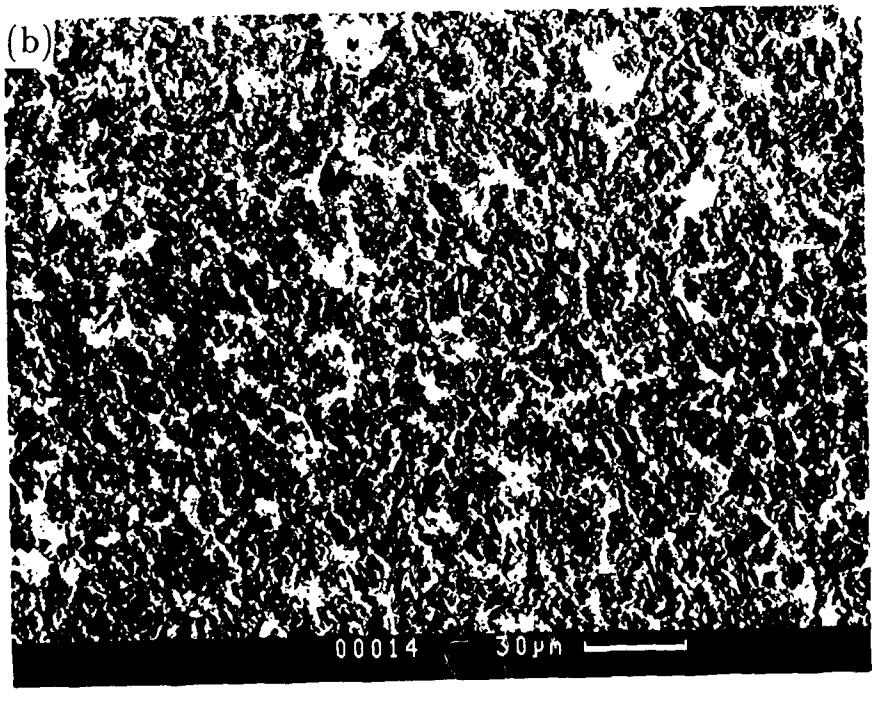

7a,b. SEM images of diamond plus Si powder. (a) Shot 807; (b) Shot 1024;

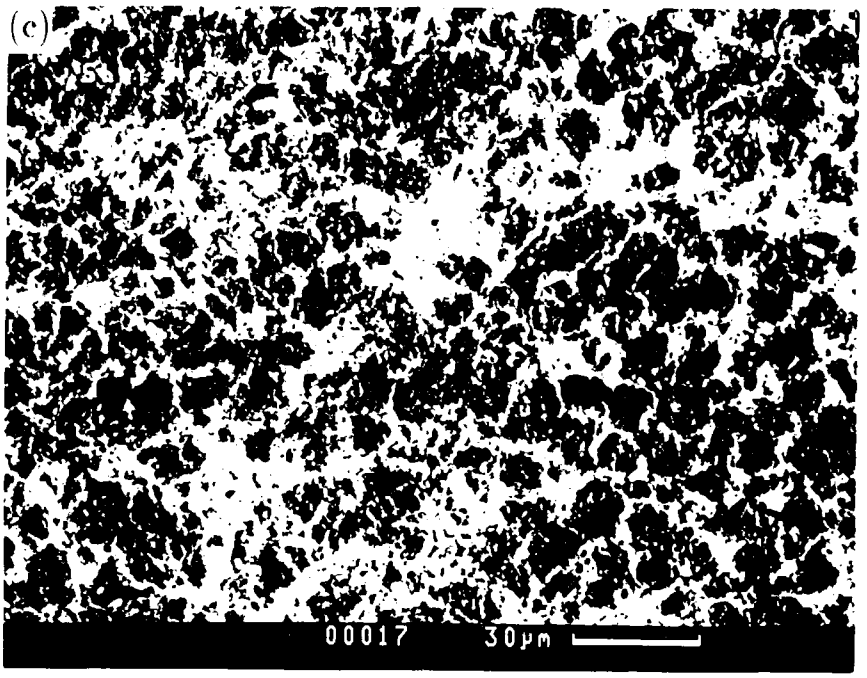

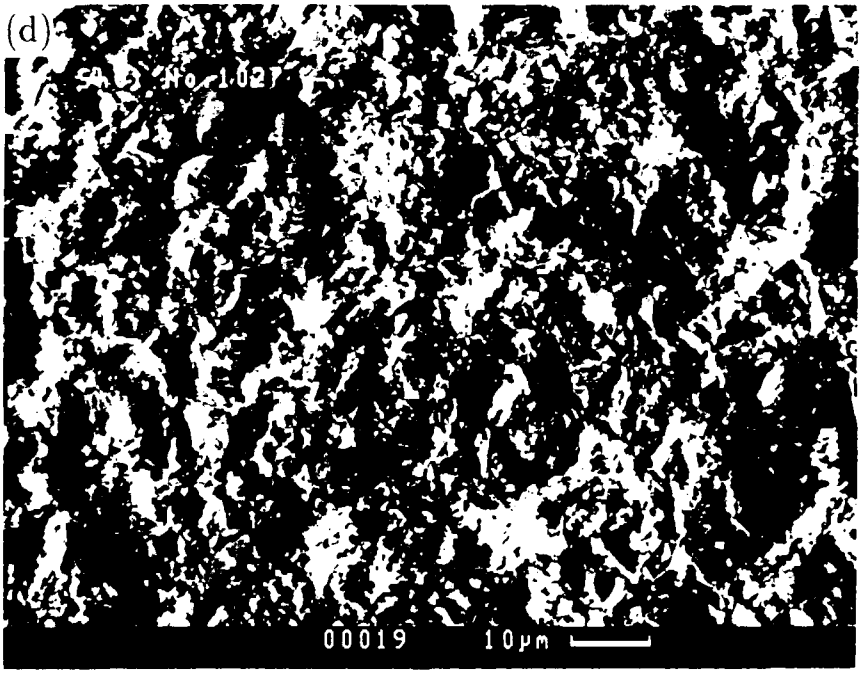

7c,d (c) Shot 1026; (d) Shot 1027;

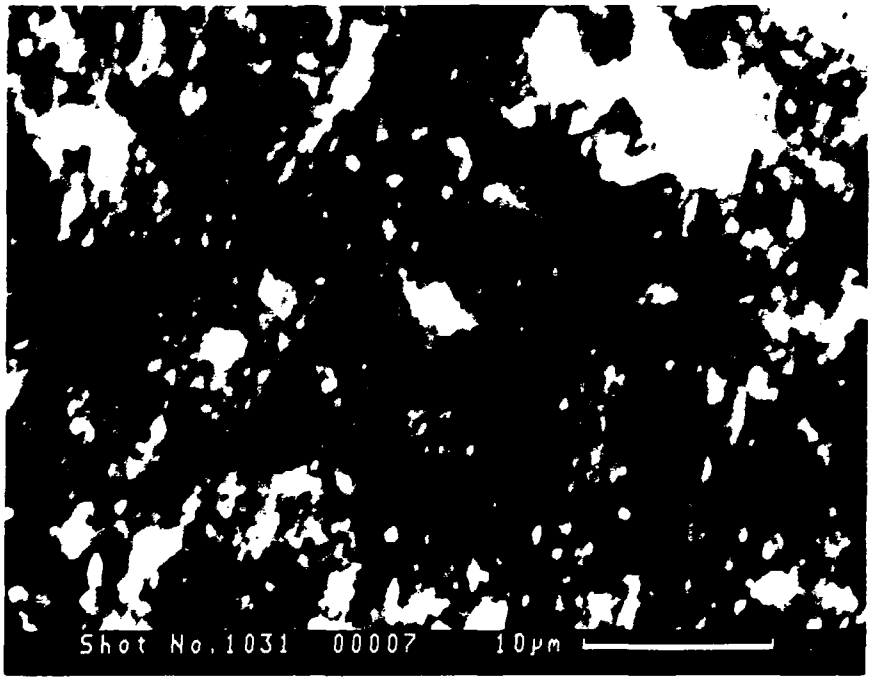

7e (e) Shot 1031. Completely melted Si gives the diamond grains a good bonding and all the diamond grains are fractured under shock loading.

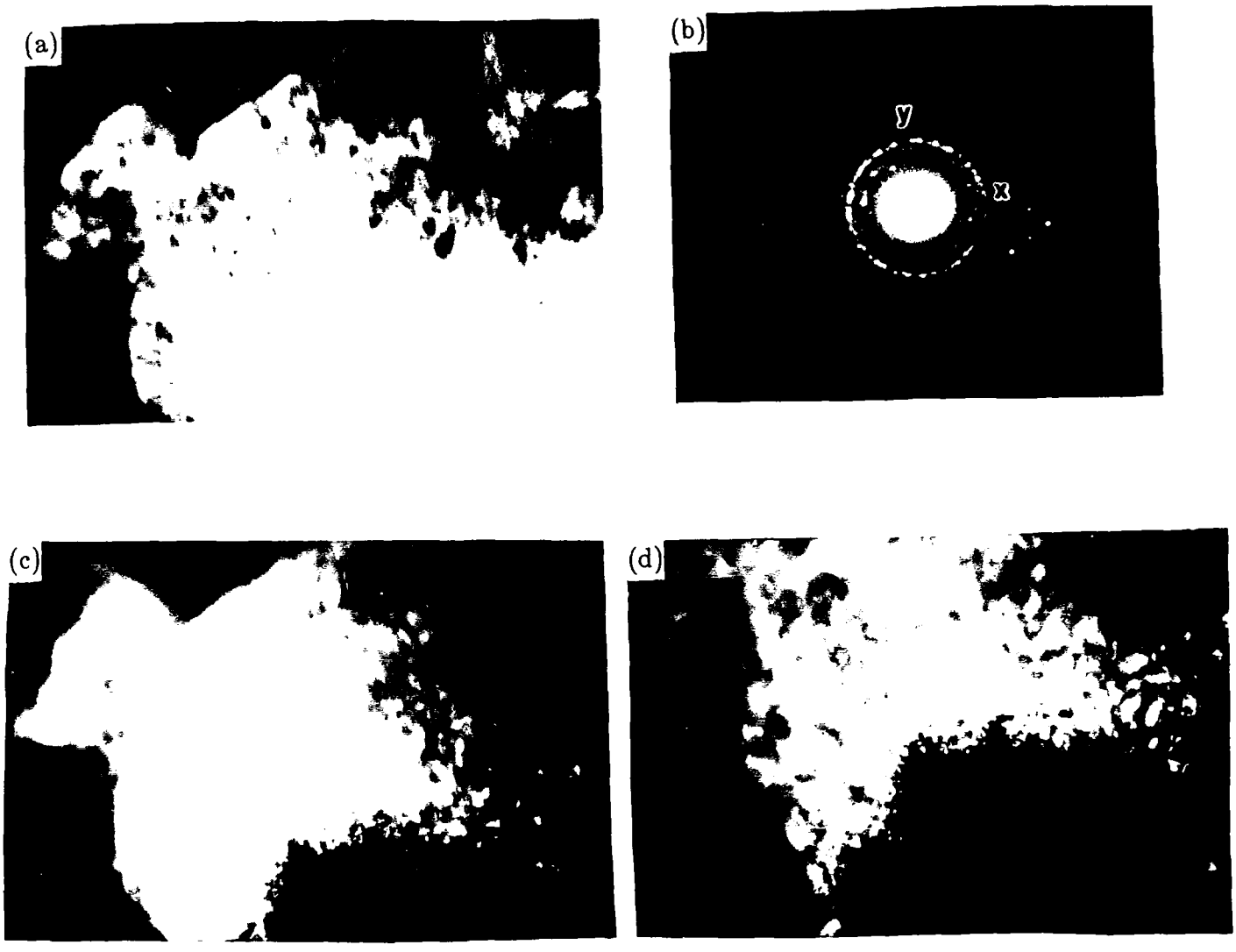

8. TEM image of Shot 983. Bright-field image (a) and diffraction pattern (b) of region of sub-micron SiC crystals; dark-field images, (c) and (d), taken for regions x and y of the diffraction pattern.

Table 7. Attempted consolidation of SCW			
Shot No.	Initial density (%)	Flyer velocity (km/s)	recovered results
998	60	1.95	recovery capsule disintegrated
1000	61	1.75	same
1004	60	1.95	small aliquot recovered

Table 8. Shock consolidation of diamond plus Si powder					
Shot No.	Mass fraction (%)		Initial density (%)	Flyer velocity (km/s)	recovered results
	Diamond	Si			
807*	95	5	60	1.18	hard, scratches glass
1024	95	5	60	1.94	harder than 807, scrathes Al_2O_3
1026	90	10	60	2.01	same
1027	95	5	60	1.90	same
1031	95	5	60	2.0	same

* sandwiched with Ti+C.

the diamond phase has not melted and recrystallized. There are no indications of reaction or solid solution between the diamond and SiC phases.

The texture of the consolidated diamond plus SCW (Fig. 9 and 10) can be seen to be somewhat different. In Fig. 10 we again see the diamond surrounded by recrystallized SiC. However, the boundaries between the diamond crystal and the SiC are less smooth than in Fig. 8, for which the SiC started out as powder rather than whisker. The diamond is not heavily deformed in the sample from this experiment and, upon tilting the TEM stage, demonstrates a clear and consistent lack of the presence of dislocations. Thus we infer that the diamond phase undergoes only elastic deformation and brittle fracture. The thermal history of the material (see below) makes it unlikely that the absence of dislocations is due to annealing. The crystal habit of the SiC material which started out as whisker can be seen to be completely different in the dark-field images (Fig. 9c and d) versus the sample where it started out as powder (Fig. 8c and d). The SCW material has recrystallized into a series of quasi-linear and coherent crystal bundles. Their dimensions are on the order of ~50 by 150nm. Moreover some open cracks ~200nm long and 10-20nm wide can be observed to terminate these bundles in Fig. 9a. We think these micro-cracks are due to the volume contraction during consolidation. The deformation features in the diamond itself are well demonstrated in Fig. 11. Just like the SEM observations, the TEM images reveal that extensive brittle (presumably crystallographically controlled) cracking is present within individual diamond grains. Moreover the crystal boundaries are not seriously deformed. The dark-field image (Fig. 11b) and the corresponding diffraction pattern (Fig. 11c) indicate that a moderate degree of streaking of the diffraction spots and microcrystalline rotation have occurred, and 100-300nm regions of the crystal have been rotated via brittle shear strains. This microcrystalline rotation is not attributed to plastic deformation followed by annealing to give dislocation-free sub-grains, because of the thermal history of the sample. The sample was shocked up to about 900K (see Table 4) by a shock wave with duration of about 1.5μs. After the shock, it was heated up to about 3000K by post-shock heating within a few *milliseccconds* (see Section 6) and then cooled down to ambient temperature in approximately the same time interval. Thus there was not enough time at high enough temperature for the dislocations to distribute themselves entirely into sub-boundaries.

We conclude from the TEM images that very little of the consolidation observed in the diamond-SiC system resulted from diamond grain boundary melting. The consolidated samples contain diamond held together with extensively melted and recrystallized β-SiC; there is no evidence to suggest plastic deformation of the diamond. The bundle fiber texture of the soundly consolidated material obtained with the recrystallized SCW versus the equant texture resulting from the melted recrystallized SiC powder gives rise to a marked difference in the resulting sample. The formation of equant microcrystallites implies that many crystal seeds were formed at the same time in the melted SiC and the SiC powder material achieved a lower temperature compared with the SCW which formed bundle-like crystallites (12). The TEM and SEM analyses indicate that we need a

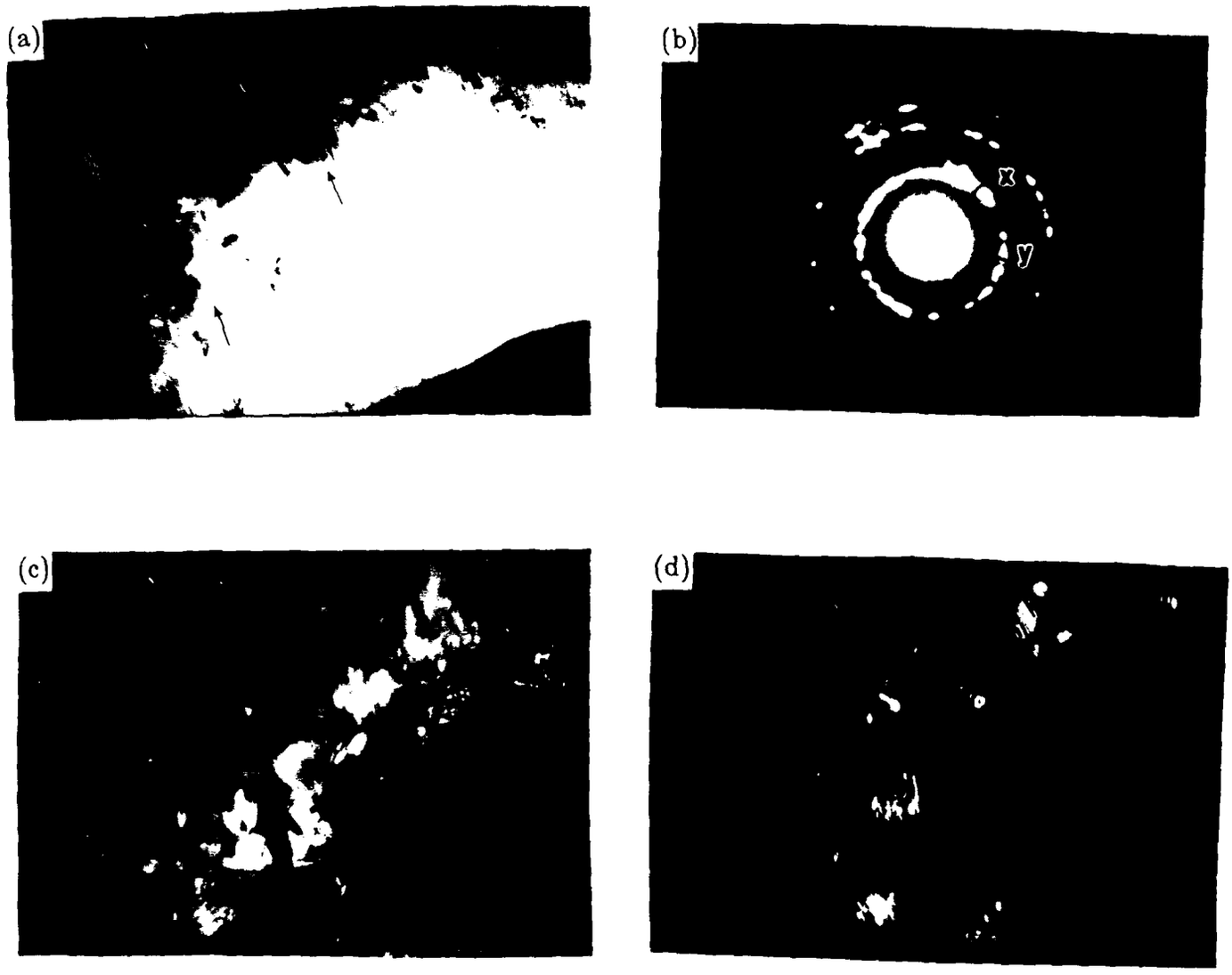

9. TEM image of Shot 973. Bright-field image (a) and diffraction pattern (b) of region of sub-micron SiC crystals observed between diamond single crystals; dark-field images, (c) and (d), taken for regions x and y of the diffraction pattern. Arrows in (a) indicate small cracks.

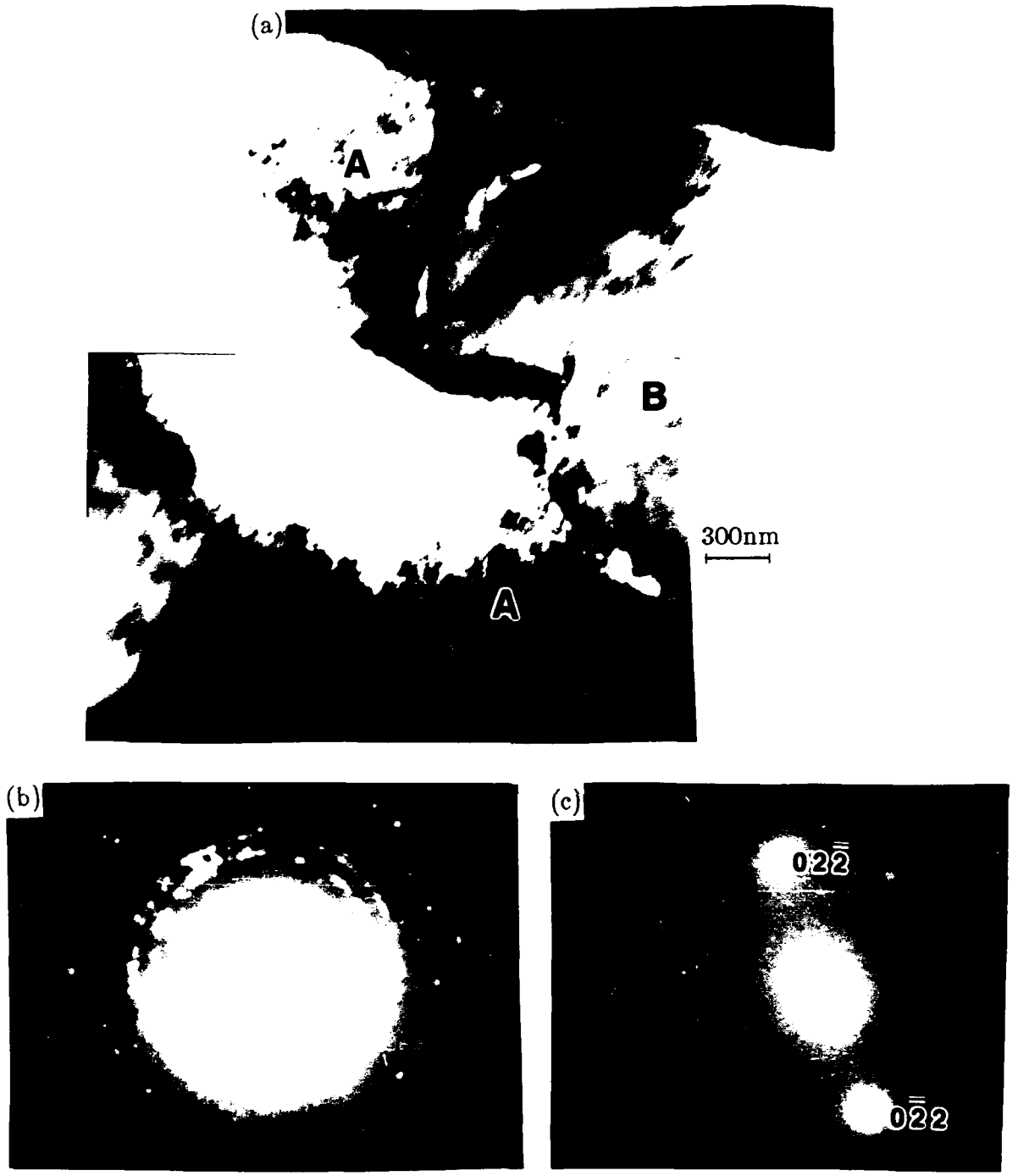

10 TEM image of Shot 973. (a) Montage showing regions of small SiC crystals (A) surrounding diamond single crystal (B); (b) and (c) diffraction patterns from regions (A) (lower) and (B) respectively.

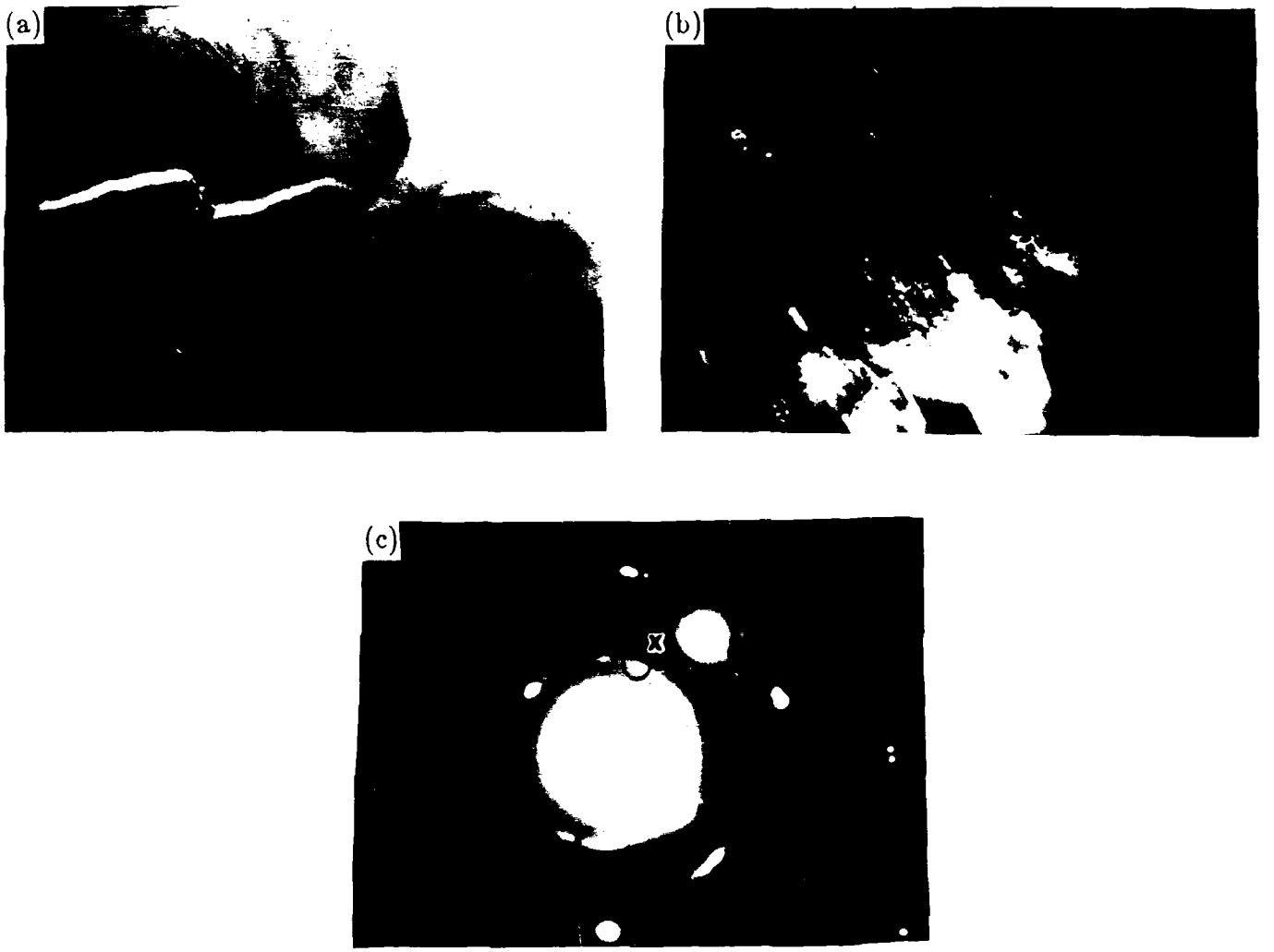

11. TEM image of Shot 767. Bright-field (a) and dark-field (b) images and diffraction pattern (c) of diamond region showing small crystals and cracking. Dark-field image taken for region x in diffraction pattern.

thermodynamic model which predicts, especially for the whiskers, virtually complete shock-induced melting of the SiC and no plastic deformation or significant melting of the diamond.

5. A New Admixture Model

Previously, in describing the thermodynamics of shock consolidation of super hard materials admixed with whiskers (7), we employed a rather standard continuum approach. We assumed the hard powder material and the whisker material could be described as having the same initial porosity. We also assumed that, upon shock loading, each phase was driven to an equal shock pressure along its individual porous Hugoniot. Our present observations, however, indicate that more melting occurs in the whisker material than is calculated from this previous model. Allowance must be made for the somewhat lower (ambient) melting points of SiC (2963K) and Si_3N_4 (2173K) as compared to diamond (4300K) and c-BN (3273K) as well as for the greater compressibility of SiC or Si_3N_4 (see reference 7, Fig. 3 and 5). As described in the previous sections, however, the contrast in melting behavior, especially for the admixtures with whiskers, appears to be considerably greater than would be expected on this basis alone.

Let us consider what takes place in admixtures of approximately cube-shaped crystals with essentially rod-like whiskers. Geometrical considerations indicate that the inherent porosity should increase when whiskers are added to the crystals. Moreover, as the length of the rods being admixed with the crystals increases relative to the size of the crystals, further increases in the porosity of the mixture are expected. Thus we infer that, in the vicinity of whiskers in the admixture, a larger effective porosity exists than in the coexisting powders. That is the whisker material will have more space in which to achieve locally a high compressional energy deposit, which is inferred to result in excess melting of the whiskers during shock consolidation.

There is extensive literature describing packing of spherical and non-spherical particles (e.g. summarized in reference 13). However no studies of the packing of cubes (like diamond or c-BN crystals) admixed with rods (like SCW) have been reported.

In order to find the relation between the porosities of whiskers and powders in the admixture, five sphere-rod packing experiments were conducted with glass spheres and rods; the experiments were designed to approximately model the present shock consolidation experiments with whiskers. Glass spheres with diameters, d_s, of 3mm and 6mm were used, while the rods were cut from long glass bars with diameters, d_r, of 0.91mm and 2mm. The glass spheres and rods were mixed and poured into a 2 liter beaker, and the bulk (total) volume of the mixture was measured after shaking.

The percent porosity ψ is

$$\psi = 100V_v/V_m \qquad (1)$$

where V_v is the volume of void space of the mixture and V_m is the total volume of the mixture. The volume percent v_r of rods is

$$v_r = 100V_{sr}/V_{sm} \tag{2}$$

where V_{sr} is the solid volume of rods and V_{sm} is the total solid volume of the mixture. It turns out that the porosity of the admixture is approximately a linear function of the volume percent of rods, v_r. Linear fits of ψ versus v_r were conducted and the results (Tables 12 to 16) are shown in Fig.12. Notably, when there are no rods mixed with the spheres (v_r=0), we observe an average porosity of 39.5%. This value is in good agreement with the loose random packing value, 39.9%, in reference 13, p. 25. The ψ-v_r relation can be expressed as

$$\psi = 39.5 + \alpha\, v_r \tag{3}$$

where α is the slope. We further find that the slope α changes linearly with the ratio of the length, l , to diameter, d_r, of the rods (Fig.13):

$$\alpha = 0.0222\, \tau - 0.0652 \qquad (R=0.992;\ 5 \leq \tau \leq 14) \tag{4}$$

where R is the linear correlation coefficient, $\tau = l\ /d_r$.

The ratio of the sphere diameter to rod diameter in our packing experiments is about 3; the ratio of the powder to whisker in consolidation ranges from 2.5 to 240. We assume that the sphere-rod packing is the same as crystal-whisker packing, and extrapolate τ in Eq. (4) to 50, which is an average value of τ for the whisker material according to the manufacturer (and also agrees with our microscopic examination). Hence, we obtain

$$\psi = 39.5 + 1.045\, v_r \tag{5}$$

If we designate ψ_s as the porosity for pure sphere packing, and ψ_r' as the excess porosity of the admixture due to the addition of rods, then ψ_s=39.5, ψ_r'=1.045v_r. Thus we have

$$\frac{\psi_r'}{\psi_s} = 0.0265\, v_r \tag{6a}$$

In our consolidation experiments, the porosity for the cube-shaped crystal-whisker mixture, ψ_m, is known, the porosity of cube-shaped crystals, ψ_p, and the porosity of whiskers, ψ_w, are unknown. Designate ψ_w' as the excess porosity of the mixture due to the addition of whiskers and assume that ψ_w' and ψ_p have the same relation as expressed in Eq. (6a), then

$$\frac{\psi_w'}{\psi_p} = 0.0265\, v_w \tag{6b}$$

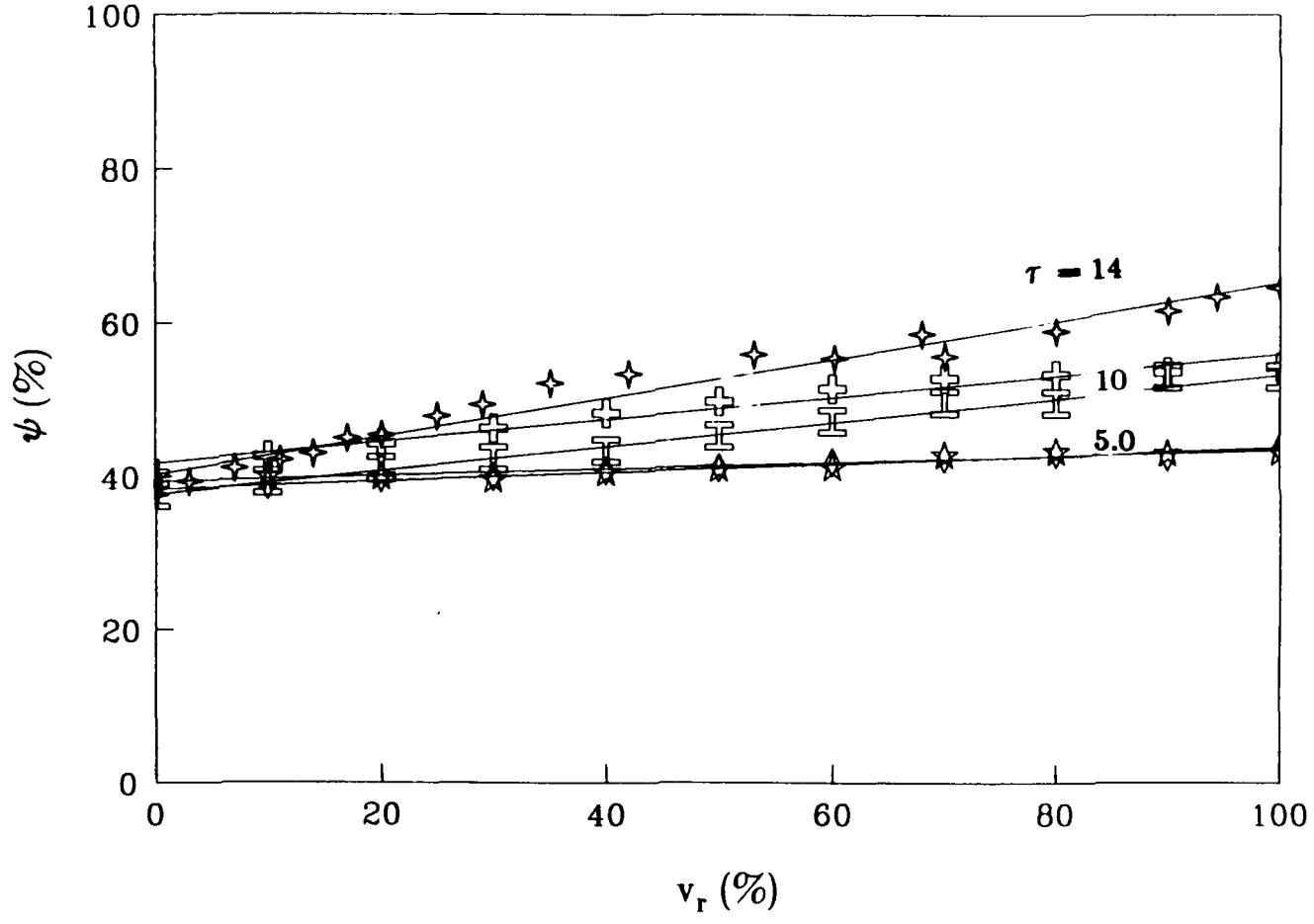

12. Results of sphere-rod packing experiments. Porosity Ψ vs. volume percent of rods v_r.✧--diameter of sphere d_S=3mm, length of rod l=12.7mm, diameter of rod d_r=O.9lmm; ✚ d_S=6mm, l=20mm,d_r=2mm; 𝕀-- d_S=3mm,l=20mm,d_r=2mm; ☆--d_S=6mm, l=lOmm, d_r=2mm; ◆ --d_S=6mm, l=lOmm, d_r=2mm.

where v_w is the volume percent of whiskers. We further assume that the porosity of whiskers, ψ_w, equals the porosity of cube-shaped crystals, ψ_p, plus the excess porosity due to the addition of whiskers, ψ_w', we obtain

$$\psi_w = \psi_p + \psi_w' \tag{7}$$

Volume conservation of the mixture and Eq. (7) yield

$$\frac{v_p}{100 - \psi_p} + \frac{v_w}{100 - (\psi_p + \psi_w')} = \frac{100}{100 - \psi_m} \tag{8}$$

Where v_p=100−v_w is the volume percent of the cube-shaped crystals in the mixture.

In Eq. (8), the first term is the fraction of the volume taken-up by particles and the second term is the fraction of volume taken-up by whiskers. With equations (6b), (7) and (8) we can calculate ψ_p, ψ_w' and ψ_w of the mixture at any initial porosity ψ_m. For example, in shot 953 (Table 1), with an initial porosity ψ_m=35%, we get ψ_p=31.7%, ψ_w'=14.8% and ψ_w=46.5%. That is the initial densities of diamond powder and SNW whisker in the mixture are 68.3% and 53.5% of their crystal densities respectively, while, in the previous model (7), both densities are assumed to be 65%.

After the porosities (or initial densities) of powders and whiskers in the admixture were obtained by the procedure outlined above, a series of thermodynamic calculations were conducted. Shock pressure, P_H, temperature, T_H, post shock temperature, T_p, and percent of material melted, L, were calculated. The results are presented in Tables 1-2, 4-5, and 9-10. The assumptions in the calculation are the same as before (7) except that the powders and whiskers have different initial densities (porosities). Details of the calculations are presented in the Appendix. The parameters used are listed in Table 11. Table 9 and Table 10 give the results of the revised calculations for the experiments described in reference 7. The new model predicts much higher shock temperatures and more melting of the whisker materials SNW and SCW. For example, for shot 936 (Table 9), our new model yields 78.1% melt and a shock temperature of 2173K (melting point) of SNW, whereas the previous model yields only 48.8% melt and 1876K. We believe that, at such high temperatures (near or at the melting point), the whisker material will lose its strength completely and change shape, either plastically or by fluid flow, to form the observed texture in the recovered sample. In contrast, the diamond and c-BN powders achieve relatively low temperatures compared with their melting points and are therefore neither plastically deformed nor extensively melted.

6. Post-Shock Heating with Ti+C

The concept of post-shock heating was first suggested by Sawaoka et al. (8). The reason we use titanium plus carbon as a heat source is that the reaction has a large reaction heat (ΔH=3037J/g (17)) and the titanium and carbon can react completely with each other under shock compression (8). Fe_2O_3 plus Al may also be a good candidate for

Table 9. Revised calculation results for c-BN plus SNW shock consolidation experiments

Experiments

Shot No.	Mass fraction (%)		Initial density (%)	Flyer velocity (km/s)	recovered results
	c-BN	SNW			
929	90.9	9.1	70	2.01	compacted
932	85	15	60	1.95	consolidated
936	85	15	71	1.94	well consolidated

Calculations

Shot No.	initial density (%)		P_H(GPa)	T_H(K)		T_p(K)		L(%)	
	c-BN	SNW		c-BN	SNW	c-BN	SNW	c-BN	SNW
929	70.8	63.1	26.8	1433 1020*	2173 1992*	1381	2173	11.0 9.6*	76.1 53.3*
932	63.3	47.4	20.1	1463 1154*	2173 2081*	1421	2173	13.3 11.3*	100 55.4*
936	73.2	61.6	25.8	1303 929*	2173 1876*	1256	2173	9.40 8.8*	78.1 48.8*

*—results from reference 7.

Table 10. Revised calculation results for c-BN plus SCW shock consolidation experiments

Experiments

Shot No.	Mass fraction (%)		Initial density (%)	Flyer velocity (km/s)	recovered results
	c-BN	SCW			
928	90.9	9.1	71	1.95	uncompacted
937	85	15	71	2.01	uncompacted
938	80	20	70	1.95	consolidated
939	75	25	71	1.97	consolidated,friable

Calculations

Shot No.	initial density (%)		P_H(GPa)	T_H(K)		T_p(K)		L(%)	
	c-BN	SCW		c-BN	SCW	c-BN	SCW	c-BN	SCW
928	71.8	64.3	26.1	1370 968*	2399 1937*	1319	2241	10.2 9.0*	28.4 19.1*
937	73.2	61.6	27.3	1352 968*	2740 1972*	1302	2561	9.9 9.3*	33.3 19.7*
938	73.8	58.7	25.3	1264 937*	2811 1834*	1218	2651	8.9 9.0*	34.8 19.2*
939	76.4	59.5	26.2	1197 895*	2829 1845*	1152	2661	8.0 8.8*	34.9 18.9*

*—results from reference 7.

Table 11. Parameters

	Diamond	c-BN	SCW	SNW
γ_o	0.9[14]	1.87[18]	1.25[20]	1.25[a]
C_o(mm/μm)	12.16[14]	10.29[18]	8.0[20]	7.90[21]
S	1.00[14]	1.25[18]	0.95[20]	1.20[21]
ρ_o(g/cm^3)	3.51[15]	3.487[15]	3.18[15]	3.18[15]
θ(K)	1600[16]	1900[16]	1140[20]	1067[b]
T_m(K)	4300[17]	3273[7]	2963[15]	2173[15]
H_m(kJ/g)	9.2[19]	9.2[19]	4.9[19]	1.081[c]

where γ_o—Grüneisen coefficient; C_o & S—constants in $D=C_o+SU$; ρ_o—crystal density;θ—Debye temperature;T_m—melting point;H_m—latent heat of melting. (a) SiC's value; (b) derived from its specific heat at 298K in reference (15); (c) estimated by assuming that it has the same entropy increase per mole upon melting as that of SiC in reference (14).

Table 12. Sphere-rod packing experimental results	
Volume percent of rods v_r(%)	porosity of mixture ψ(%)
0.0	37.6
3.0	39.3
7.0	41.1
11.0	42.2
14.0	43.0
17.0	45.0
20.0	45.4
25.0	47.8
29.0	49.3
35.0	52.1
42.0	53.3
53.0	55.8
60.2	55.3
68.0	58.5
70.0	55.6
80.0	58.9
90.0	61.5
94.4	63.3
100	64.5
Note: d_s=3mm, d_r=0.91mm, l =12.7mm, r=14.	

Table 13. Sphere-rod packing experimental results	
Volume percent of rods v_r(%)	porosity of mixture ψ(%)
0.0	37.6
10.0	39.4
20.0	41.1
30.0	42.3
40.0	43.4
50.0	45.2
60.0	47.2
70.0	49.6
80.0	49.6
90.0	53.0
100	53.0
Note: d_s=6mm, d_r=2mm, l =20mm, r=10.	

Table 14. Sphere-rod packing experimental results	
Volume percent of rods v_r(%)	porosity of mixture ψ(%)
0.0	37.9
10.0	38.8
20.0	39.7
30.0	39.9
40.0	40.8
50.0	41.1
60.0	41.8
70.0	42.3
80.0	43.0
90.0	42.5
100	43.7
Note: d_s=3mm, d_r=2mm, l =10mm, r=5.	

Table 15. Sphere-rod packing experimental results	
Volume percent of rods v_r(%)	porosity of mixture ψ(%)
0.0	40.0
10.0	40.2
20.0	40.1
30.0	39.7
40.0	40.6
50.0	41.1
60.0	41.3
70.0	42.9
80.0	43.4
90.0	43.1
100	43.3
Note: d_s=6mm, d_r=2mm, l =10mm, r=5.	

Table 16. Sphere-rod packing experimental results	
Volume percent of rods v_r(%)	porosity of mixture ψ(%)
0.0	40.4
10.0	42.7
30.0	46.3
40.0	48.3
50.0	49.8
60.0	51.4
70.0	52.8
80.0	53.3
90.0	53.6
100	54.3
Note: d_s=3mm, d_r=2mm, l =20mm, r=10.	

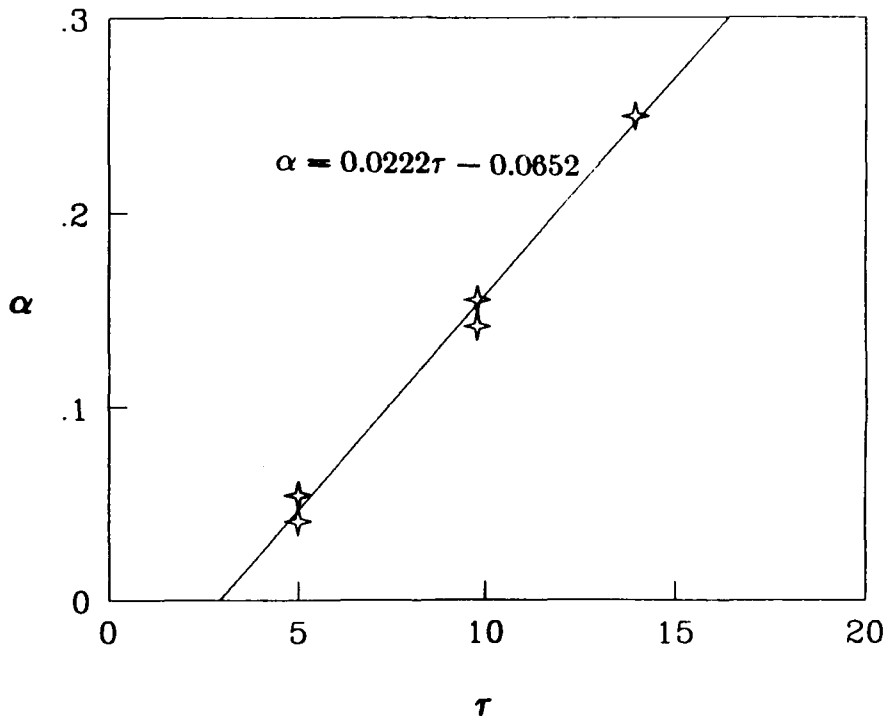

13. Slope α of the ψ-v_r relation in Fig. 12 vs. τ. The fit shows a linear correlation coefficient of 0.992.

post-shock heating (its reaction heat is about 4000J/g when completely reacted), but Boslough has studied this reaction under shock-wave loading and pointed out that reaction under shock maybe be incomplete (22).

The Ti powder we used has a size range of 1-3μm and is mixed with carbon black in a stoichiometric ratio. The reaction equation is

$$Ti + C = TiC$$

If T is the post-shock temperature of the product TiC, the energy balance equation is

$$\Delta H + E_H = \int_{300}^{T} C_p \, dT + L \, \Delta H_m \tag{9}$$

where E_H is the Hugoniot energy, C_p is the specific heat of TiC (17), L is the melting fraction of TiC, and the latent heat ΔH_m of melting of TiC is 1187J/g (17). The Hugoniot energy is dependent on the shock pressure and the initial state of Ti+C. If the crystal specific volume V_{oc} of TiC is used as an approximation of the Hugoniot specific volume, then E_H is given approximately as

$$E_H = \frac{1}{2} P_H (V_{oo} - V_{oc}) \tag{10}$$

where V_{oo} is the initial specific volume of Ti+C, and V_{oc} equals 0.2025cm^3/g (12).

If ϕ is the initial fractional porosity, E_H can be expressed as

$$E_H = \frac{1}{2} P_H V_{oc} \frac{\phi}{1 - \phi} \tag{11}$$

With Eq. (9) and (11), we get the $T - P_H$ relation at different values of ϕ. For example, for ϕ=40%, the reaction heat itself will heat the TiC to its melting point (3293K) and melt 48.5% of it when P_H=0; when P_H=9.05GPa, the TiC will be completely melted. Some calculation results are illustrated in Fig. 14. It is clear that the higher the pressure or the greater the initial porosity, the higher the post-shock temperature that the TiC will reach. That is more heat will be released from TiC.

In the shock consolidation, the post-shock heating is probably very important, especially in the comparatively low pressure range. Successful shock compaction is probably impossible under low pressure without post-shock heating, for the following reasons. Under low pressure, very little melt can be obtained and this will not be sufficient to bond the particles together. The relatively low shock pressure also implies that the brittle particles will not be able to change their shape plastically to give a dense compact. In addition, the rapid cooling of the sample will induce cracks. In the case of post-shock heating via the Ti+C=TiC reaction, the sample is able to cool slowly and thus eliminate the formation of cracks due to rapid cooling, and remove residual stresses. The post-shock heating can also heal the cracks induced during the pressure release process and possibly also remove voids from the sample via conventional sintering action. Shot 808

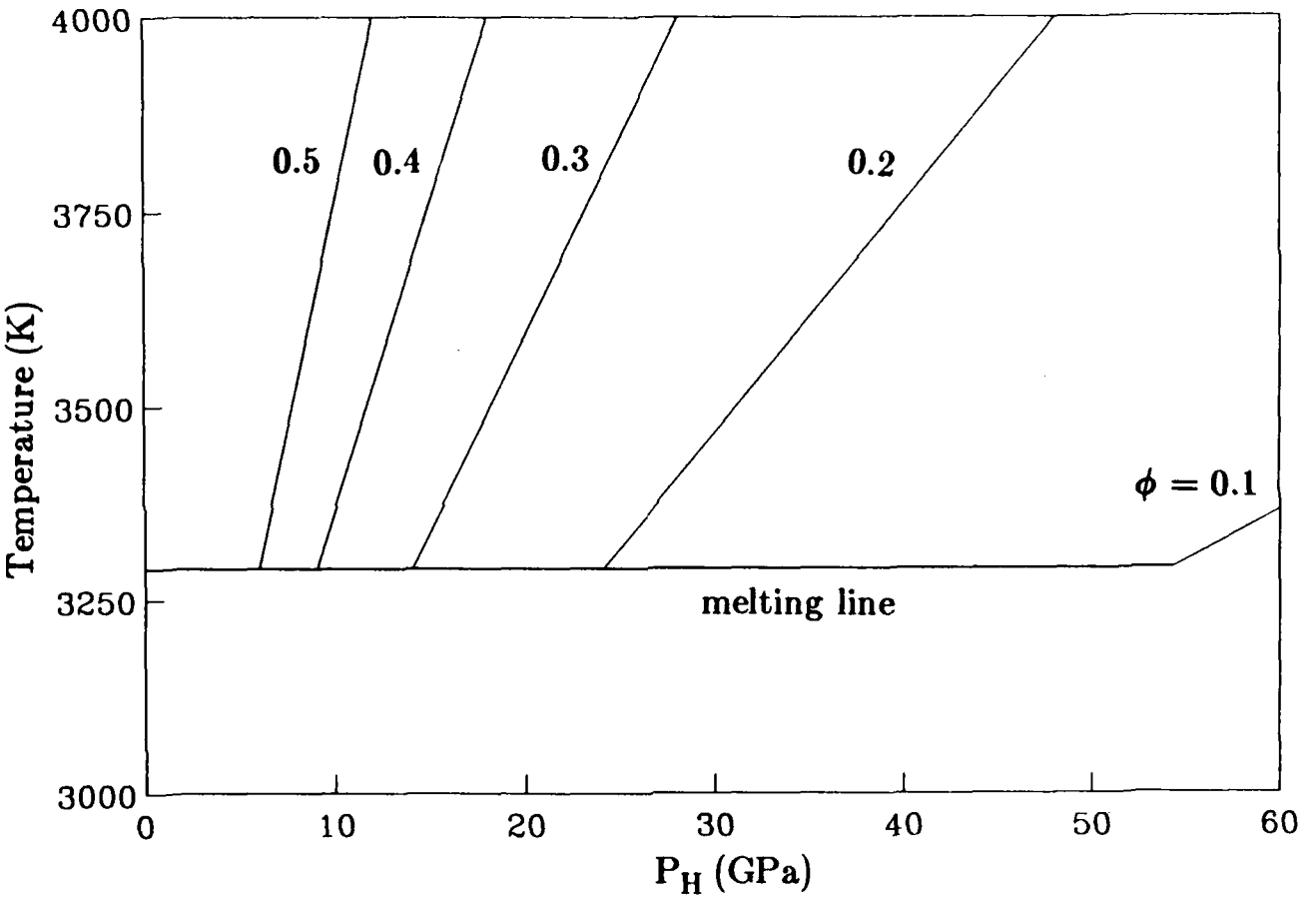

14. Post-shock temperature of TiC vs. shock pressure P_H at different initial porosity (ϕ). Melting line shown is appropriate for TiC.

(see Table 5) was conducted without Ti+C. The flyer velocity is 1.36km/s (almost the same as shot 786). The recovered sample is uncompacted. These two shots exemplify the importance of post-shock heating of the sample by TiC formation.

As an example, we calculated the time dependent temperature profiles of shot 766 (Table 4, Fig. 16), for the geometry shown in Fig. 15. We assumed that, after shock loading, the sample, TiC and stainless steel 304 (S.S.304) capsule are each at their crystal density, and that the heat flow is one dimensional. We chose a typical initial sample thickness of 2mm, but varied the thickness of TiC (0.25-1.0mm).

To solve the one dimensional heat equation, a finite differential numerical method was employed (23). The thermal diffusivities used here are: $4\times10^{-6}m^2/s$ (S.S.304) (24), $10^{-4}m^2/s$ (diamond) (7), $5\times10^{-6}m^2/s$ (SCW) (7). For simplicity, a constant specific heat of 0.4J/gK (24) was assumed for S.S.304. The Debye specific heat model was used for diamond (Debye temperature, 1860K) (see Table 11) and SCW (Debye temperature, 1140K) (see Table 11). To simplify the calculation further, we chose the thermal diffusivity of TiC as infinite. The post-shock temperature rise of S.S.304 was omitted for it is small (20). The calculation results are shown in Fig. 16. Calculations were performed for four different thicknesses of TiC. We can see from Fig. 16 that a thicker TiC layer gives the sample a higher average temperature. In Fig. 16d, an average temperature of 3000K (higher than the melting point (2963K) of SCW) was obtained and the SCW in the sample must be melted in this case. In Fig. 16b, with a TiC thickness of 0.5mm which corresponds to 0.83mm porous Ti+C, the average temperature of the sample reached 2370K, which is 80% of the melting point of SCW. It is known that the carbides will lose their brittleness at a temperature 80-90% of their melting points (25). So we infer that SCW will be efficiently annealed in this case. The optimum thickness for this proposed process is approximately 0.8 to 1.7mm when the initial porosity of Ti+C is 40%, under a shock pressure of 10GPa which is typical of these experiments. The porous Ti+C thicknesses we used in the present experiments were 0.8-1.5mm, which are very close to what we infer is optimum from the calculations.

7. Discussion and Conclusion

The shock wave consolidation mechanism in an admixture of a superhard powder and a whisker material is the melting and recrystallizing of the whisker material. Rod-like whiskers result in excess porosity in the mixture, and deformation and melting are both enhanced by this excess porosity. We note that the whisker materials have lower melting temperature and strength as compared with diamond or c-BN powder. In contrast, when fine SiC powder is admixed with sphere-like diamond or c-BN powder, it fills the voids between the particles and no excess porosity can be obtained. Thus the fine SiC powder results in lower post-shock temperatures upon shock consolidation and therefore is not suitable as an additive material. Our new admixture model of powder plus whisker provides a physically based model of the experimental results.

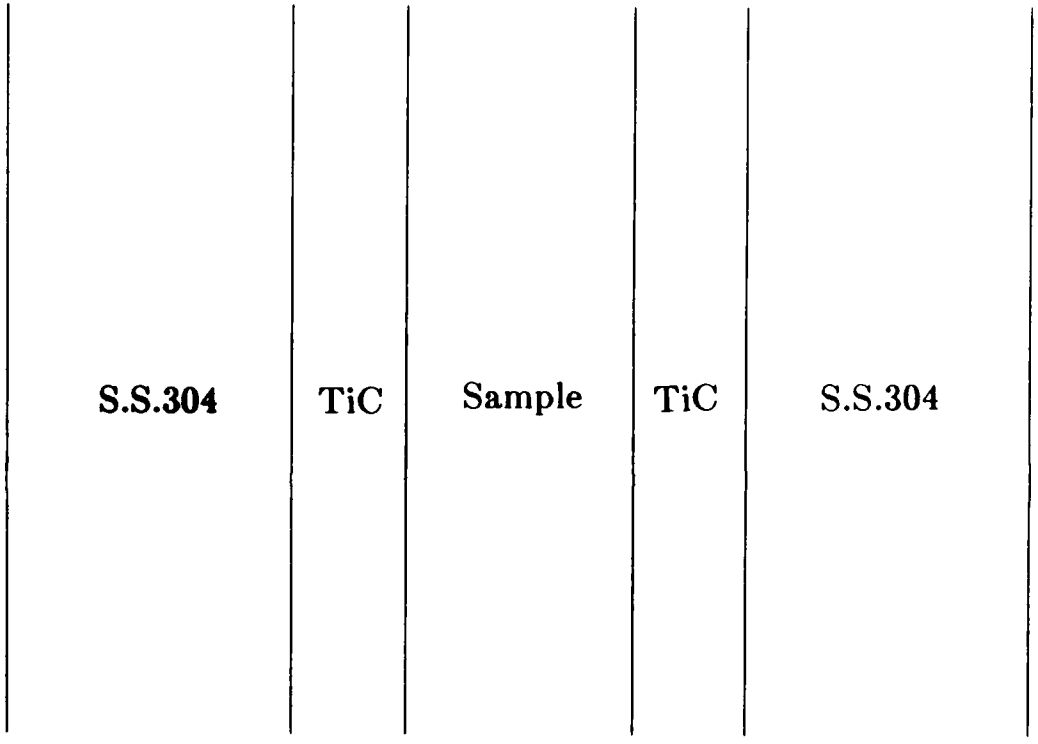

15. Geometry assumed in calculation of post-shock heating.

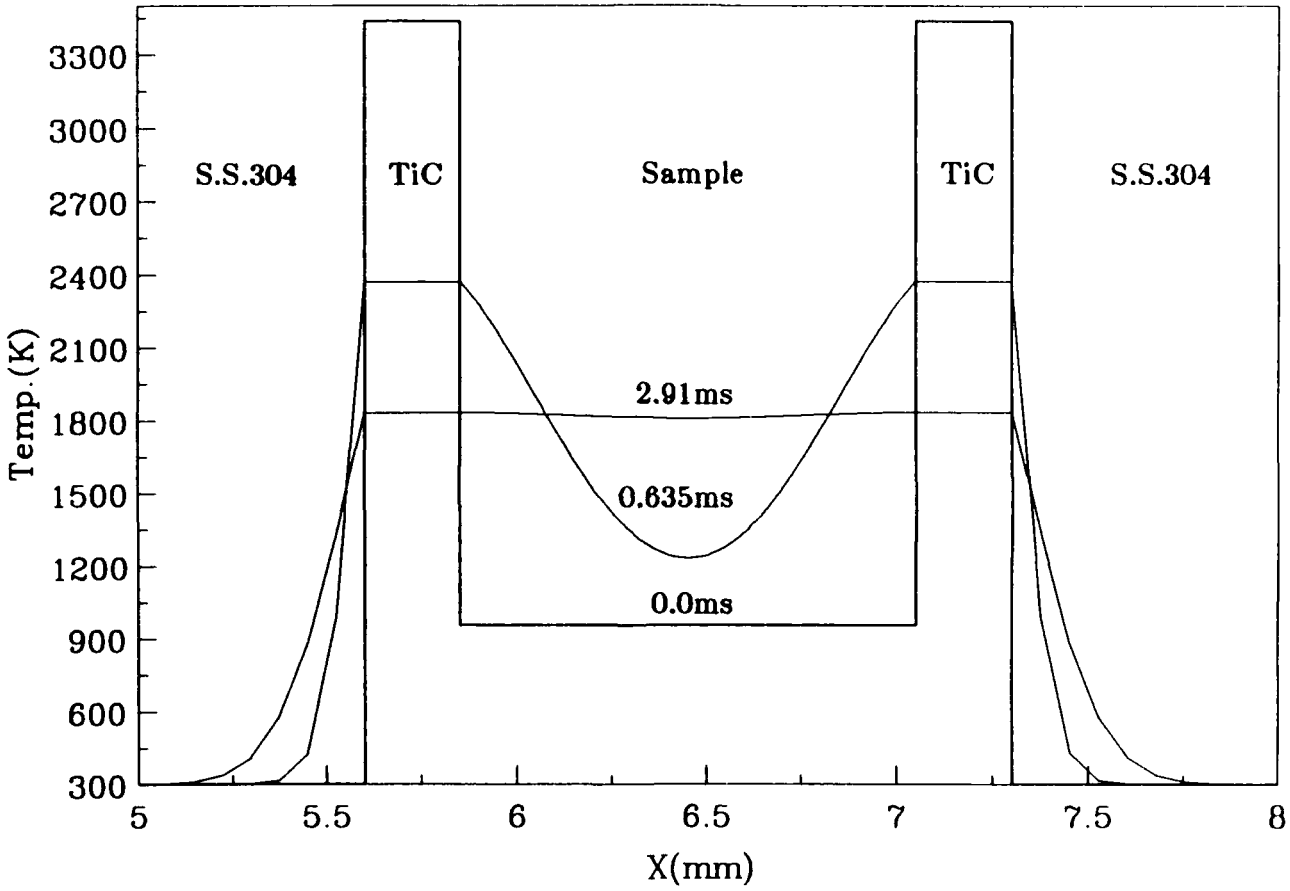

16a. Calculated temperature profiles of post shock heating. (a) The thickness of TiC is 0.25mm, the average temperature of the sample reaches 1819K at 2.91ms;

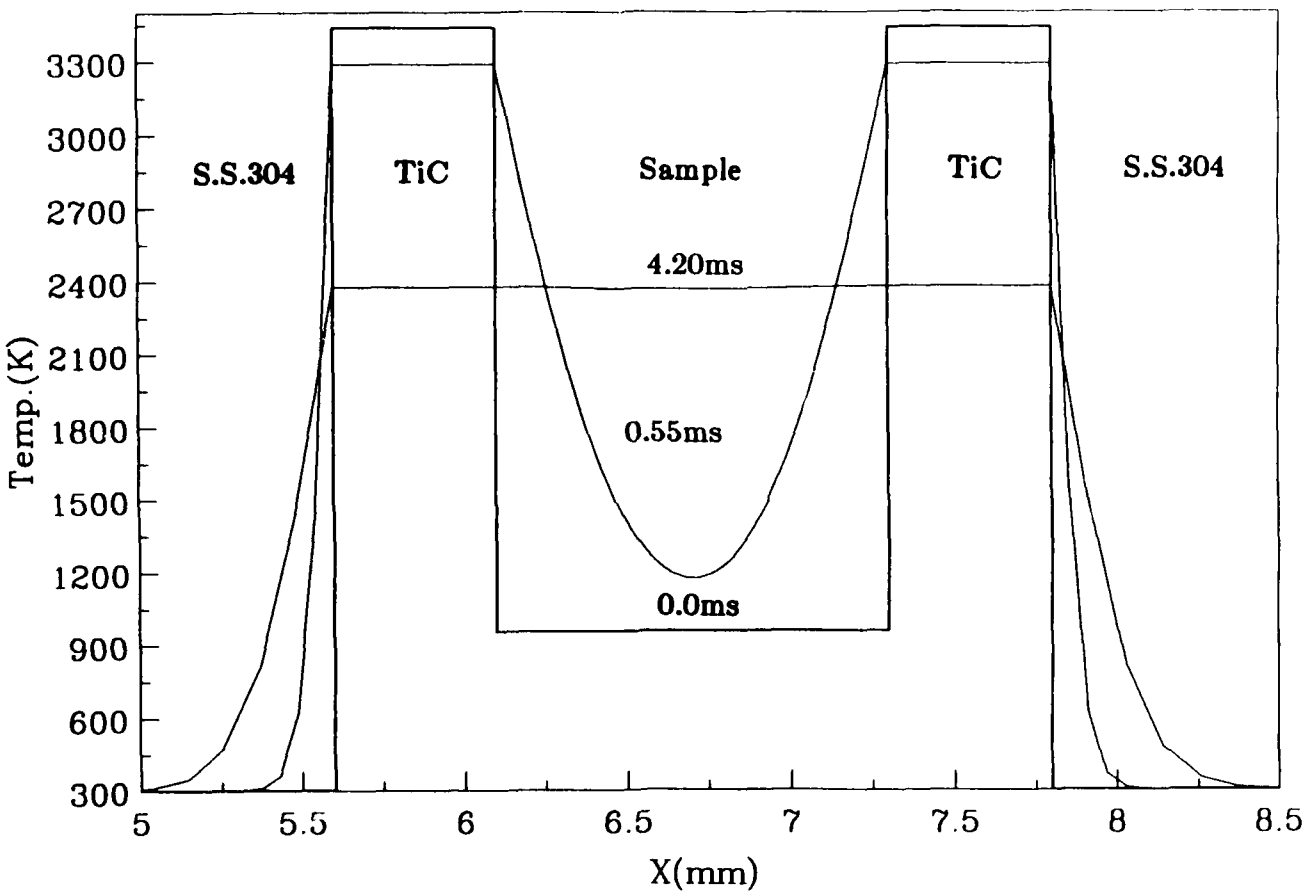

16b. (b) TiC 0.5mm thick, average temperature 2370K at 4.20ms;

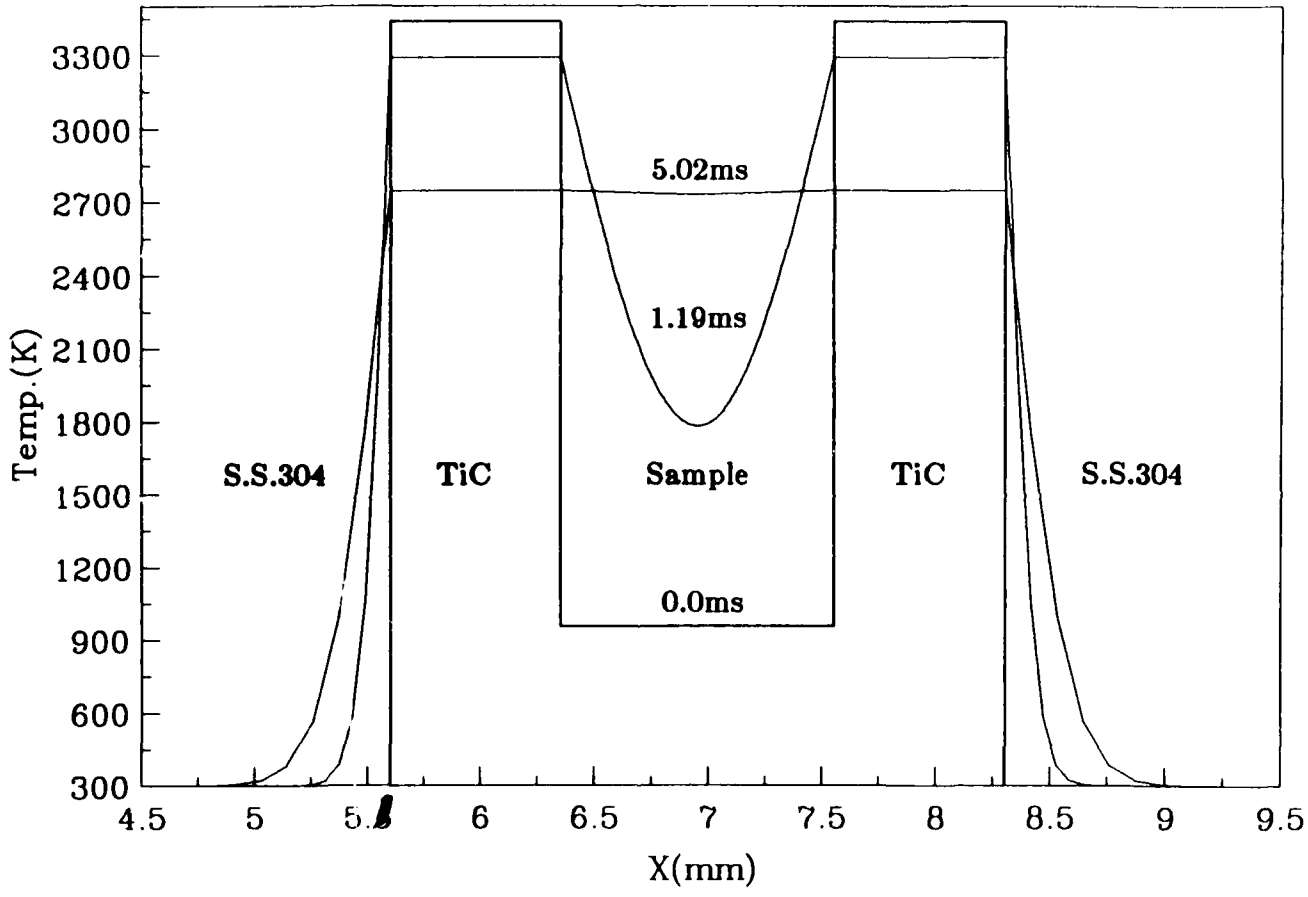

16c. (c) TiC 0.75 thick, average temperature 2737K at 5.02ms;

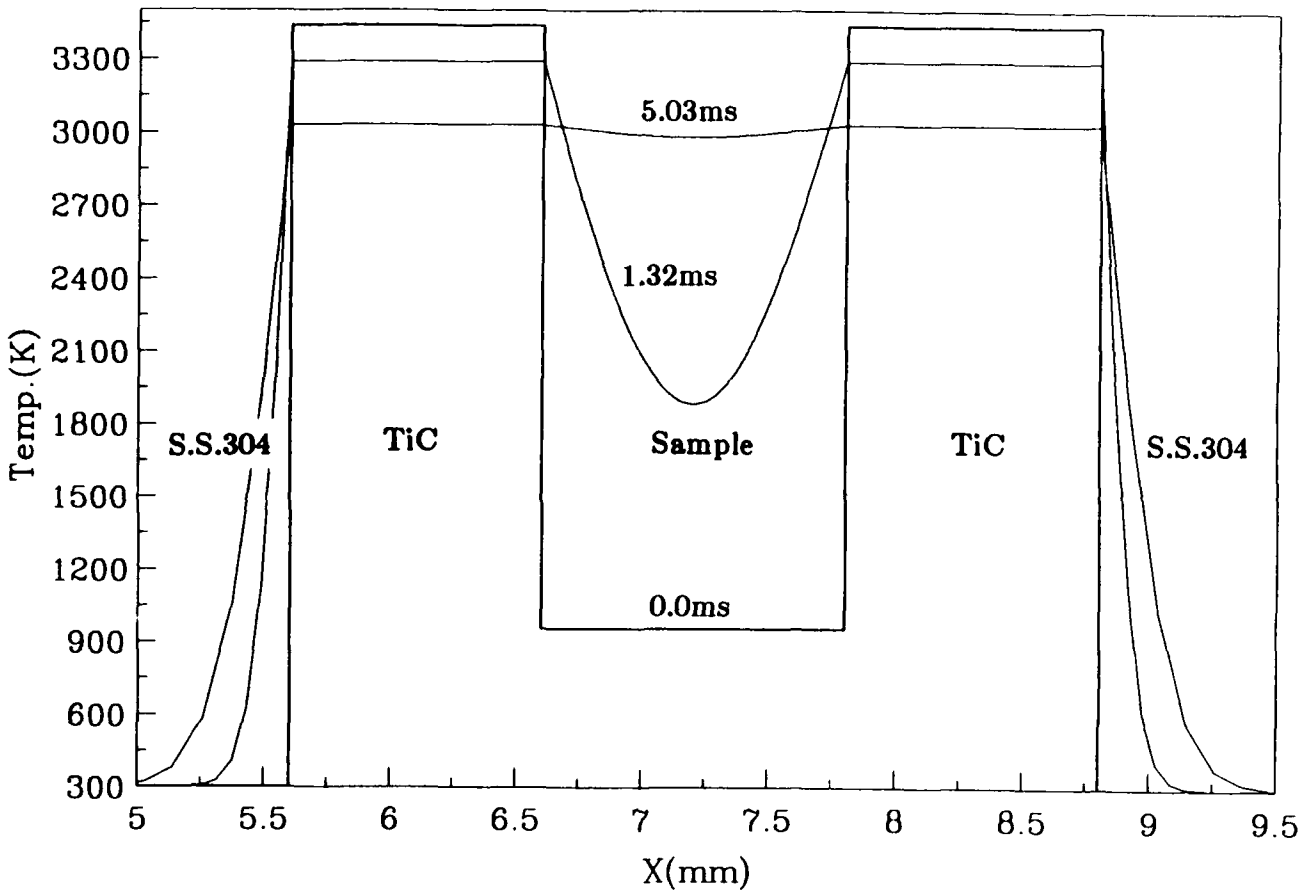

16d. (d) TiC 1.Omm thick, average temperature 3000K at 5.03ms.

The effect of post-shock heating obtained from the reaction Ti+C=TiC is very important in consolidation under low dynamic pressure. Very well consolidated samples composed of c-BN plus SCW were obtained with the post-shock heating technique for shock compaction at a pressure of 12GPa.

Pulverization of synthetic diamond crystals during shock loading occurs in most of our experiments. It may be impossible to obtain a practically useful compact if this problem is not solved. In comparison, c-BN single crystals appear to be unaffected by shock loading when admixed with whisker material.

The SNW material, because of its reaction with carbon under high temperature and pressure, is not suitable for shock compaction when mixed with diamond powder; the SCW yields better compacts.

The commercially obtained Si powder ($<44\mu$m) shows some promise as a beneficial additive in consolidation of diamond. Well consolidated diamond samples were obtained with 5% or 10% Si. Further work needs to be conducted in this area.

It appears, at present, that c-BN plus SCW is the most promising material to obtain practically useful superhard polycrystalline compacts via shock consolidation.

LIST OF PUBLICATIONS

W. Yang, G. M. Bond, H. Tan, T. J. Ahrens, and G. Liu (1990) Dynamic consolidation of super hard materials, submitted to J. Materials Research

LIST OF OF PARTICIPATING SCIENTIFIC PERSONNEL

Wenbo Yang, Lindhurst Laboratory of Experimental Geophysics, Seismological Laboratory, California Institute of Technology, Pasadena, CA 91125

G. M. Bond, Department of Materials and Metallurgical Engineering, New Mexico Institute of Mining and Technology, Socorro, NM 87801

Hua Tan, present address: Beijing Institute of Technology, P. O. Box 327, Beijing, People's Republic of China

G. Liu, Department of Materials and Metallurgical Engineering, New Mexico Institute of Mining and Technology, Socorro, NM 87801

References

1. D. K. Potter and T. J. Ahrens, Appl. Phys. Lett. 51, 317-319 (1987).
2. F. P. Bundy and R. H. Wentorf, J. Chem. Phys. 38, 1144-1149 (1963).
3. T. Akashi, V. Lotrich, A. Sawaoka and E. K. Beauchamp, J. Amer. Ceram. Soc. 68, c-322-c-324 (1985).
4. T. J. Ahrens and D. K. Potter, in Shock Waves in Condensed Matter-1987 edited by S. C. Schmidt and N. C. Holmes (North-Holland Physics Publishing, Amsterdam, the Netherlands,1988), pp. 419-422.
5. S. Sawai and K. Kondo, J. Am. Ceram. Soc. 71, c-185-c-188 (1988).
6. T. Akashi, A. B. Sawaoka, Shock compaction of cubic boron nitride powders, J. Mater. Science 22, 1127-1134 (1987).
7. H. Tan and T. J. Ahrens, Dynamic consolidation of cubic boron nitride and its admixtures, J. Mater. Res. 3, 1010-1020 (1988).
8. A. Sawaoka and T. Akashi, in Shock Waves in Condensed Matter-1987, edited by S. C. Schmidt and N. C. Holmes (North-Holland Physics Publishing, Amsterdam, the Netherlands, 1988), pp. 423-425.
9. JANAF Thermodynamical Tables, edited by M. W. Chase et al (American Chemical Society and the American Institute of Physics for the National Burean of Standards, 1985), p. 1563, 634.
10. P. Kumar and R. J. Clifton, J. Appl. Phys. 48, 4850-4852 (1977).
11. LASL Shock Hugoniot Data, edited by S. P. Marsh (University of California, Berkeley, CA, 1980), p. 328, 249.
12. R. W. Heine, C. R. Loper, Jr. and P. C. Rosenthal, Principles of Metal Casting (McGraw-Hill BooK Company, 1967), pp. 178-209.
13. D. J. Cumberland and R. J. Crawford, Packing of Particles (Elsevier Science Publishers B. V., Amsterdam, The Netherlands, 1987), p. 25.
14. M. N. Pavlovskii, Soviet Physics-Solid State 13, 741-742 (1971).
15. Tateho Chemical Industries Co.,Ltd., Technical data, 1988.
16. T. Soma, A. Sawaoka and S. Saito, Synthesis of Dense Form Boron Nitride and Diamond by Shock Compression, in Proceedings of the Forth International Conference on High Pressure-1974, Special issue of the Review of Physical Chemistry of Japan, edited by J. Osugi (Kawakita, Kyoto, Japan, 1975), pp. 446-453.
17. LANGE's HANDBOOK OF CHEMISTRY, edited by J. A. Dean (McGraw-Hill, Inc., 1985), p. 3-2, 9-63, 9-137, 4-123.

18. E. Knittle, R. M. Wentzcovitch, R. Jeanloz & M. L. Cohen, Experimental and theoretical equations of state of cubic boron nitride, Nature 337, 349-352 (1989).

19. J. A. Van Vechen, Phys. Rev. B7, 1479-1507 (1973).

20. R. Kinslow, High Velocity Impact Phenomena (Academic Press, Inc., New York, 1970), p. 549, 551, 374.

21. Derived from T. Mashimo's data in " Shock Yielding Properties of Brittle Materials ", in Shock Waves in Condensed Matter-1987, edited by S. C. Schmidt and N. C. Holmes (North-holland Physics Publishing, Amsterdam, the Netherlans, 1988), pp. 289-292.

22. M. B. Boslough, A Thermaldynamical Model for Shock-Induced Chemical Reactions in Porous Solids: Analogs and Contrasts to Detonation, in Proceedings of the Ninth Symposium (International) on Detonation-1989.

23. J. M. Hill and J. N. Dewynne, Heat Conduction (Blackwell Scientific Publications, 1987), p. 197.

24. J. H. Lienhard, A Heat Transfer Text Book (Prentice-Hall, Inc., Englewood Cliffs, N. J., 1981), p. 492.

25. P. Schwarzkopf and R. Kieffer, Cemented Carbides (The Macmillan Company, 1960), p. 67.

26. T. J. Ahrens, in Methods of Experimental Physics (Academic, New York, 1987), Vol.24, Part A, pp. 185-234.

27. T. J. Ahrens, D. Kostka, P. Kasiraj and T. Vreeland, Jr., in Rapid Solidification Processing Principles and Technologies,III,Proceedings of the Third Conference on Rapid Solidification Processing, edited by R. Mehrabian (U.S. National Bureau of Standards, Gaithersburg, MD, 1982), pp. 672-677.

28. W. H. Gourdin, J. Appl. Phys. 55, 172-181 (1984).

29. R. B. Schwarz, P. Kasiraj, T Vreeland, Jr. and T. J. Ahrens, Acta Metall. 32, 1243 (1984).

30. R. a. Babie, B. S. Hemingway and J. R. Fisher, Thermodynamic Properties of Minerals and Related Substances at 298.15K and 1bar (10^5 pascals) Pressure and at Higher Temperatures (Geological Survey Bulletin 1452, 1978), p. 41.

Appendix

A. Shock Pressure P_H

The impedance match technique (26) was used to calculate the shock pressure in the sample from the measured flyer velocity and the sample Hugoniot estimated below.

From the Grüneisen equation of state, we can get the porous Hugoniot on the P-V plane (see Figure A) as

$$P_H = \frac{P_d\left(\frac{V_{od}-V_d}{2} - \frac{V_d}{\gamma}\right)}{\frac{V_\infty - V_d}{2} - \frac{V_d}{\gamma}} \tag{1A}$$

in which V/γ = constant is assumed.

With the porous Hugoniot obtained from Eq.(1A), the mixture Hugoniot is obtained on the basis of volume additivity at constant pressure (20).

For convenience of calculation of the shock pressure, we use the shock relations

$$U_s = V_\infty [\, P_H/(V_\infty - V_d)\,]^{\frac{1}{2}} \tag{2A}$$

$$U_p = [\, P_H(V_\infty - V_d)\,]^{\frac{1}{2}} \tag{3A}$$

to obtain the linear relation $U_s = C_o + SU_p$ (reference 26).

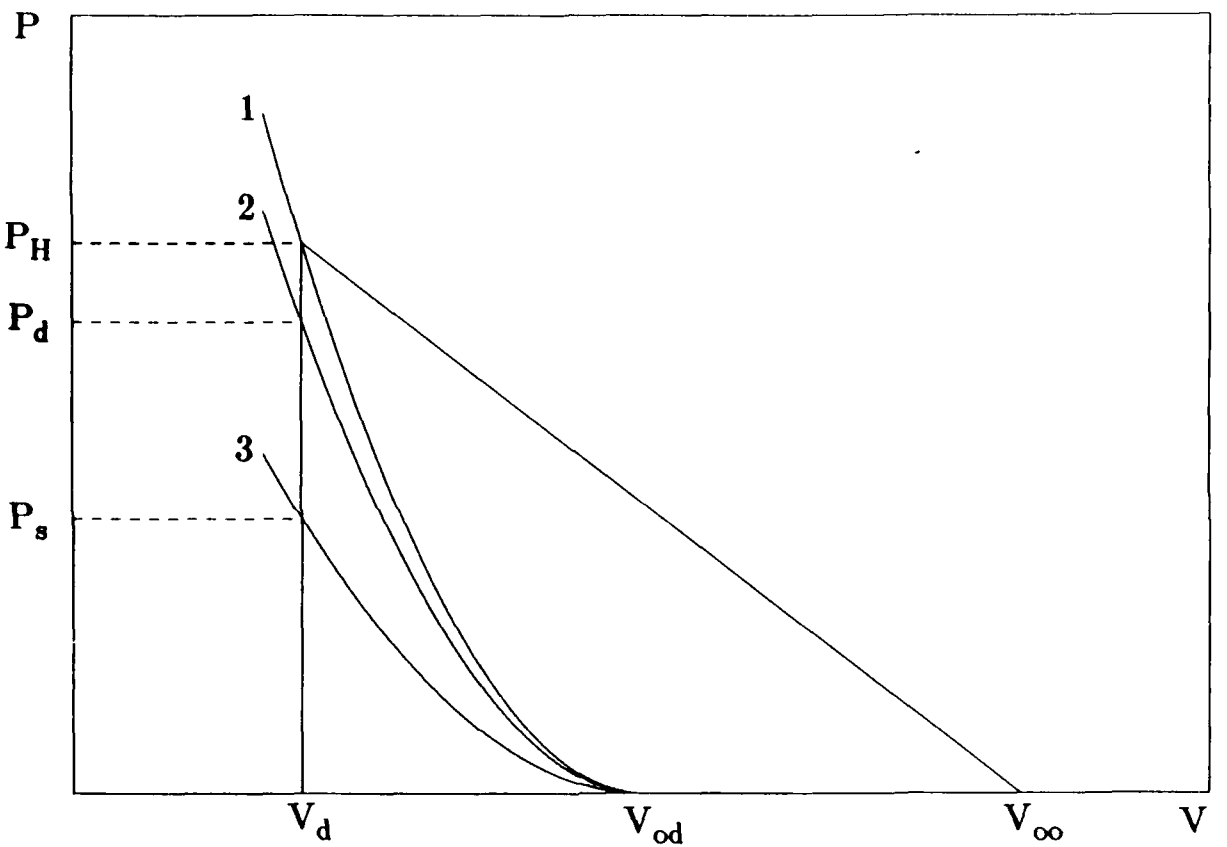

A. P-V plane. Curves 1, 2 and 3 are porous Hugoniot, known Hugoniot centered at V_{od} and adiabat, respectively.

The Hugoniot data used for c-BN, Diamond and SiC are from references 11, 14 and 20, respectively.

B. Calculation of continuum shock temperature T_H

The continuum shock temperature T_H of each constituent is calculated by the method of reference (26)

$$\int_{T_s}^{T_H} C_v dT = E_H - E_s \tag{4A}$$

where C_v is the Debye specific heat. The Hugoniot energy and isentropic energy are

$$E_H = \frac{1}{2} P_H (V_\infty - V) \tag{5A}$$

$$E_s = -\int_{V_{od}}^{V} P_s dV \tag{6A}$$

The isentropic pressure P_s and temperature T_s are

$$P_s = -\rho_o C_o^2 \exp(\gamma\eta) \int_o^\eta [(\gamma - S)x - 1] / [\exp(\gamma x)(1 - Sx)^3] dx \tag{7A}$$

$$T_s = T_o e^{\gamma\eta} \tag{8A}$$

where $\eta = 1 - V/V_o$.

C. Calculation of the post shock temperature T_p

Assuming each constituent release along its Hugoniot curve to V_{od}, the post shock temperature T_p is given by the following equations

$$\int_{T_o}^{T_p} C_v dT = \frac{1}{2} P_H (V_\infty - V_H) - \int_{V_H}^{V_{od}} P_H dV \tag{9A}$$

$$P_H = C_o^2 \eta / [V_{od}(1 - S\eta)^2] \tag{10A}$$

D. Melting fraction L

The formula used to calculate melt fraction is (27-29)

$$L \leq \frac{P_H (V_\infty - V_{od})}{2[C_p (T_m - T_o) + H_m]} \tag{11A}$$

where C_p is the specific heat, T_m and H_m are the melting point and latent heat of fusion, respectively.